1968

The x-ray crystal structure determination of Fe3(CO)11P(C6H5)3 and the design, installation, and automation of a neutron diffraction system

Donald James Dahm
Iowa State University

68-10,457

DAHM, Donald James, 1941-

THE X-RAY CRYSTAL STRUCTURE DETERMINATION OF $Fe_3(CO)_{11}P(C_6H_5)_3$ AND THE DESIGN, INSTALLATION, AND AUTOMATION OF A NEUTRON DIFFRACTION SYSTEM.

Iowa State University, Ph.D., 1968
Chemistry, physical

University Microfilms, Inc., Ann Arbor, Michigan

THE X-RAY CRYSTAL STRUCTURE DETERMINATION OF $Fe_3(CO)_{11}P(C_6H_5)_3$ AND THE DESIGN, INSTALLATION, AND AUTOMATION OF A NEUTRON DIFFRACTION SYSTEM

by

Donald James Dahm

A Dissertation Submitted to the

Graduate Faculty in Partial Fulfillment of

The Requirements for the Degree of

DOCTOR OF PHILOSOPHY

Major Subject: Physical Chemistry

Approved:

Signature was redacted for privacy.

In Charge of Major Work

Signature was redacted for privacy.

Head of Major Department

Signature was redacted for privacy.

Dean of Graduate College

Iowa State University
Ames, Iowa

1968

TABLE OF CONTENTS

THE X-RAY CRYSTAL STRUCTURE DETERMINATION OF $Fe_3(CO)_{11}P(C_6H_5)_3$

Introduction

Since 1930, when iron tetracarbonyl was found to be trimeric, the configuration of $Fe_3(CO)_{12}$ has been highly disputed. The i.r. spectra of solutions of $Fe_3(CO)_{12}$ contain strong terminal carbonyl absorption bands around 2000 cm^{-1}, but only very weak bridging carbonyl bands around 1800 cm^{-1} (1, 2). In 1957, work in this laboratory on the solid-state i.r. spectrum of $Fe_3(CO)_{12}$ strongly indicated the existence of the bridging carbonyls (3). Most configurations proposed recently for $Fe_3(CO)_{12}$ have had both terminal and bridging carbonyls (4, 5), although some authors have suggested configurations containing no bridging carbonyls (1, 6). A crystal structure determination attempted by earlier workers in this laboratory showed the iron atoms to be arranged triangularly (7), but unfortunately disorder prevented a complete structural determination. Later, when Mossbauer-effect studies indicated that $Fe_3(CO)_{12}$ contains two iron atoms having identical electronic environments with the third having a more symmetrical environment, a linear model regained favor (4, 5).

Subsequently a different arrangement of the carbonyls, the first shown in Figure 1, was proposed on the basis of

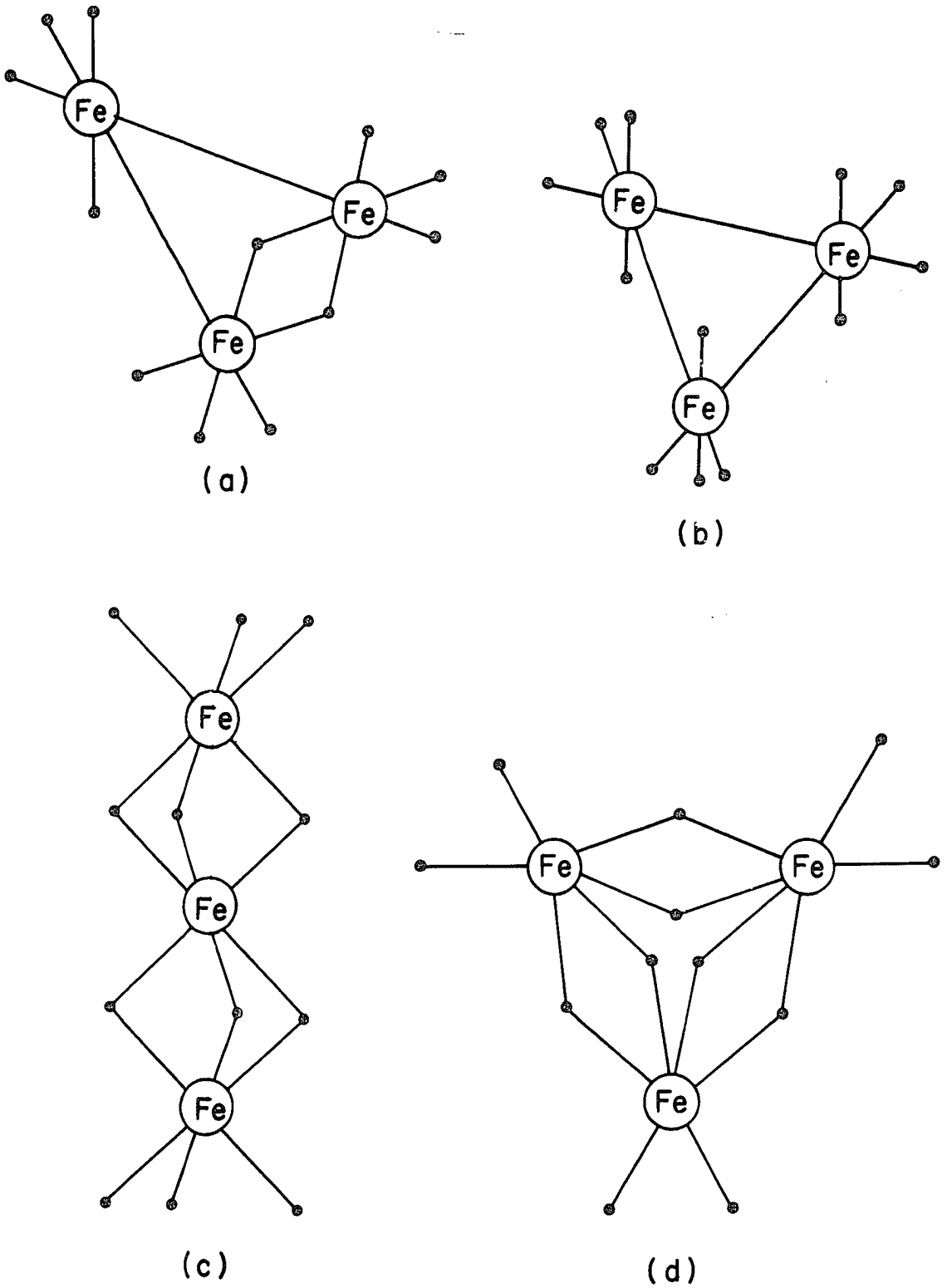

Figure 1. Proposed structures for $Fe_3(CO)_{12}$

the crystal structure determination (8) of $HFe_3(CO)_{11}^-$ which could explain this disparity. However $HFe_3(CO)_{11}^-$ is not a derivative of $Fe_3(CO)_{12}$ and the two have vastly different physical properties. Therefore it is difficult to assess the degree of disparity between the two structures.

A derivative of $Fe_3(CO)_{12}$, namely $Fe_3(CO)_{11}P(C_6H_5)_3$, was prepared and came to our attention. We felt a structural study of this derivative might well give better evidence for the exact arrangement of the iron and carbonyl groups in $Fe_3(CO)_{12}$ than studies of its own disordered crystal. If the structure of $Fe_3(CO)_{11}P(C_6H_5)_3$ is used to infer the structure of $Fe_3(CO)_{12}$, these two substances should have very similar properties. Crystals of both compounds are green-black, and their solutions are dark green. Solutions of both show intense i.r. terminal C-O absorption bands and weak bridging C-O bands. Both compounds show much more intense bridging C-O absorptions in the solid state than in solution. These facts (9) strongly indicate that $Fe_3(CO)_{12}$ and $Fe_3(CO)_{11}P(C_6H_5)_3$ have very similar structures. Therefore, we decided to undertake the x-ray crystal structure determination of $Fe_3(CO)_{11}P(C_6H_5)_3$.

After the molecular configuration of $Fe_3(CO)_{11}P(C_6H_5)_3$ became obvious from this determination, we prepared a communication (10) dealing with the implications of the

structure of $Fe_3(CO)_{11}P(C_6H_5)_3$ for that of $Fe_3(CO)_{12}$. In that paper it was asserted that the configuration of $Fe_3(CO)_{12}$ was similar to that of $HFe_3(CO)_{11}^-$, that the bridged iron-iron distance was 2.55, that the unbridged iron-iron distance was 2.68, and that the carbonyl bridges would be asymmetrically located. These distances differed somewhat from those found (8) for $HFe_3(CO)_{11}^-$ and differed considerably from those reported on the basis of the original x-ray work (7) done on $Fe_3(CO)_{12}$. On the basis of the $HFe_3(CO)_{11}^-$ configuration, symmetric carbonyl bridges had been proposed (8).

However, before our communication was published, we were informed of a new structure determination of $Fe_3(CO)_{12}$. This redetermination (11) indicated our proposed distances were very good; due to the disorder, any asymmetric nature of the carbonyl bridges was undetected in that study. For this reason, we believe the structure of $Fe_3(CO)_{11}P(C_6H_5)_3$ is the best evidence for the structure of $Fe_3(CO)_{12}$ available to date.

Experimental

$Fe_3(CO)_{11}P(C_6H_5)_3$ was prepared by Angelici and Siefert (9) by the reaction of $Fe_3(CO)_{12}$ and $P(C_6H_5)_3$. They obtained dark green, plate-like single crystals by evaporation of a pentane solution. Since these crystals were reported to decompose in the atmosphere, they were

placed in thin-walled, Lindemann glass capillaries.

Preliminary precession photographs (Cu K_α) showed the unit cell to be monoclinic with systematic absences: $\underline{hk\ell}$ when $\underline{h} + \underline{k} \neq 2n$, and $\underline{h0\ell}$ when $\underline{\ell} \neq 2n$. These absences are consistent with either space group C_s^4 - C_c or C_{2h}^6 - $C_{2/c}$. The unit cell parameters at 25° are $\underline{a}$ = 37.14 ± 0.03, $\underline{b}$ = 12.26 ± 0.01, and $\underline{c}$ = 26.05 ± 0.02 Å, and β = 93.96 ± 0.15°. These parameters and their standard deviations were obtained by averaging several reflection positions (Mo Kα radiation, λ = 0.7107 Å) whose centers were determined by left-right, top-bottom beam splitting on a previously aligned General Electric single crystal orienter. Since this compound is either soluble or decomposes in common solvents, its density was not measured but was estimated to be about 1.6 ± 0.2 g/cc. There, however, is no real need to measure the density in order to determine the number of molecules in the unit cell. From chemical knowledge, it is obvious that the molecule cannot contain any elements of symmetry from either of the possible space groups; therefore all atoms must be in general positions. This means that the number of molecules in the unit cell must be four or some integer multiple of four. The calculated densities corresponding to these possibilities are:

0.41, 0.83, 1.24, 1.66, 2.07 ... g/cc

of which 1.66 is the only reasonable value for a compound of this type, indicating 16 molecules per unit cell.

For data collection a crystal, having approximate dimensions 0.06 x 0.35 x 0.19 mm along the a, b, and c crystal axes respectively, was mounted such that the b axis was along the axis of the capillary and hence along the spindle axis.

Data were collected at room temperature with Zr-filtered, Mo Kα radiation utilizing a General Electric XRD-5 x-ray unit equipped with a goniostat and scintillation counter. Within a 2θ sphere of 35°, peak heights of all reflections were checked visually on a ratemeter. Beyond 35°, several reflections were spotchecked to verify that there were exceedingly few reflections in this range which could be classified as "observed". This had been expected because of the rapid fall off in intensities at higher angles observed on the photographs. About 1800 reflections from one octant were found to be significantly above background; their intensities were measured using a one hundred second, θ-2θ coupled scan (1.67° in 2θ) using a take-off angle of 1°.

Individual background values were obtained from a plot of measurements of background versus 2θ. Intensities were further corrected for Lorentz and polarization factors, streak due to non-characteristic radiation, and crystal

decomposition. Errors in intensities were determined as previously described (12).

Because of the small crystal size (0.004 mm^3) and the relatively small linear absorption coefficient (16 cm^{-1}), no corrections for lost counts, extinction, or absorption were felt necessary. Since all the recorded reflections were at rather low 2θ values, the maximum x-ray path length through the crystal was only slightly more than the intermediate crystal dimension. The intensity of the 0k0 reflections showed little variation with respect to the rotation of the phi axis, also indicating that absorption was not significant.

Structure Determination

A Patterson function was computed from sharpened data (13) and a vector which was assumed to be an iron-iron vector resulting from the c-glide, a symmetry element present in both possible space groups, was located on the Harker line. A superposition employing the minimum function was then carried out and readily revealed the positions of two thirds of the iron atoms in the unit cell; in addition the presence of a center of symmetry in the unit cell was also indicated. This, together with an equivalent result obtained via a statistical test (14), strongly suggested that the correct space group is $C_{2/c}$, as was later confirmed by the successful refinement in this

space group. Using these iron positions and the centric space group, the remaining atoms were found by successive structure factor and electron density map calculations.

The presence of sixteen molecules in a unit cell with space group of order eight requires that each asymmetric unit contain two crystallographically independent molecules. Therefore there are 264 independent, non-hydrogen, positional parameters and the associated thermal parameters to be refined. Consequently, our first approach was to use a block-diagonal technique in an attempt to refine the structural parameters. However, satisfactory convergence did not result, probably due to the neglect of large interaction terms between adjacent atoms in this monoclinic space group. A full matrix program was then employed, varying all the parameters of each molecule in alternating cycles. Refinement resulted in convergence with $R = \Sigma||Fobs|-|Fcalc||/\Sigma|Fobs| = 0.106$ for all atoms isotropic and $R = 0.078$ with the iron and phosphorus atoms anisotropic. The corresponding values of the weighed discrepancy factor,

$$wR = (\Sigma w(|Fobs|-|Fcalc|)^2/\Sigma w(Fobs)^2)^{1/2}$$

are 0.131 and 0.091 respectively. The parameters resulting from this refinement are shown in Tables 1 and 2.

Least squares refinement was also carried out by correcting for both the real and imaginary parts of anomalous dispersion and treating all benzene rings as

Table 1. Positional and anisotropic thermal parameters for heavy atoms with their standard errors

Atom	AFe1	AFe2	AFe3	AP	BFe1	BFe2	BFe3	BP
x/a	0.39557	0.42346	0.46659	0.04950	0.29930	0.23622	0.25364	0.33332
Error	0.00018	0.00017	0.00018	0.00031	0.00018	0.00019	0.00020	0.00034
y/b	0.21255	0.41642	0.25298	0.08001	0.03183	0.09838	0.17358	-0.07677
Error	0.00058	0.00055	0.00057	0.00107	0.00059	0.00067	0.00068	0.00116
z/c	0.35052	0.36164	0.35953	0.12939	0.14239	0.09435	0.18433	0.09596
Error	0.00027	0.00025	0.00027	0.00043	0.00026	0.00027	0.00029	0.00048
β_{11}	0.00081	0.00063	0.00078	0.00052	0.00060	0.00088	0.00082	0.00074
Error	0.00008	0.00007	0.00008	0.00012	0.00007	0.00008	0.00008	0.00014
β_{22}	0.00458	0.00472	0.00448	0.00537	0.00600	0.00865	0.01078	0.00639
Error	0.00073	0.00071	0.00069	0.00131	0.00076	0.00090	0.00092	0.00144
β_{33}	0.00173	0.00149	0.00165	0.00118	0.00184	0.00190	0.00208	0.00151
Error	0.00016	0.00014	0.00016	0.00027	0.00016	0.00017	0.00018	0.00029
β_{12}	-0.00018	0.00014	0.00004	-0.00036	-0.00002	0.00087	0.00099	0.00011
Error	0.00019	0.00019	0.00020	0.00036	0.00022	0.00023	0.00024	0.00039

Table 1. (Continued)

Atom	AFe1	AFe2	AFe3	AP	BFe1	BFe2	BFe3	BP
β_{13}	0.00011	0.00001	-0.00002	-0.00002	-0.00011	-0.00029	-0.00011	-0.00011
Error	0.00008	0.00008	0.00008	0.00014	0.00008	0.00009	0.00009	0.00015
β_{23}	-0.00031	0.00003	0.00023	0.00039	-0.00017	-0.00084	-0.00108	-0.00061
Error	0.00029	0.00029	0.00030	0.00053	0.00039	0.00033	0.00036	0.00056

Table 2. Light atom positional and thermal parameters and their errors

Atom	X/a	Error	Y/b	Error	Z/c	Error	B	Error
AB C1	0.4518	(12)	0.3597	(40)	0.4144	(19)	6.5	1.5
AB 01	0.4658	(8)	0.3745	(25)	0.4576	(12)	6.8	0.9
AB C2	0.4557	(12)	0.3652	(40)	0.3104	(19)	6.4	1.5
AB 02	0.4618	(7)	0.3791	(24)	0.2649	(11)	5.4	0.9
AT1C1	0.3984	(12)	0.2191	(41)	0.4171	(20)	7.3	1.5
AT101	0.3963	(8)	0.2246	(29)	0.4643	(14)	8.5	1.1
AT1C2	0.3952	(13)	0.0777	(55)	0.3505	(18)	6.9	1.5
AT102	0.3996	(9)	-0.0232	(36)	0.3535	(13)	9.4	1.2
AT1C3	0.3484	(16)	0.2257	(44)	0.3455	(18)	7.6	1.6
AT103	0.3183	(11)	0.2427	(32)	0.3422	(13)	9.8	1.2
AT2C1	0.3912	(12)	0.4408	(37)	0.3999	(16)	5.0	1.3
AT201	0.3643	(9)	0.4582	(27)	0.4246	(12)	7.8	1.0
AT2C2	0.3978	(12)	0.4473	(40)	0.3063	(18)	6.4	1.5
AT202	0.3792	(8)	0.4702	(26)	0.2684	(12)	7.4	1.0
AT1C4	0.3985	(12)	0.2198	(42)	0.2846	(21)	6.4	1.6
AT104	0.3982	(8)	0.2187	(25)	0.2385	(13)	6.6	0.9
AT3C1	0.4721	(11)	0.1673	(40)	0.4103	(18)	5.4	1.4
AT301	0.4758	(9)	0.1052	(32)	0.4468	(13)	8.9	1.1
AT3C2	0.5115	(13)	0.2851	(37)	0.3616	(17)	4.6	1.3
AT302	0.5434	(9)	0.2996	(26)	0.3624	(11)	7.1	1.0
AT3C3	0.4692	(13)	0.1586	(51)	0.3160	(22)	8.2	1.7
AT303	0.4705	(7)	0.0872	(29)	0.2831	(12)	7.0	0.9
BB C1	0.2161	(14)	0.0693	(42)	0.1553	(18)	6.9	1.5
BB 01	0.1890	(9)	0.0233	(28)	0.1717	(12)	7.9	1.0
BB C2	0.2545	(13)	0.2455	(50)	0.1236	(19)	7.4	1.6
BB 02	0.2612	(8)	0.3352	(31)	0.1016	(12)	8.4	1.1
BT1C1	0.3182	(13)	0.1468	(48)	0.1208	(18)	6.5	1.6
BT101	0.3364	(9)	0.2142	(31)	0.1003	(12)	7.8	1.0
BT1C2	0.2720	(13)	-0.0672	(47)	0.1600	(17)	6.4	1.5
BT102	0.2556	(9)	-0.1461	(31)	0.1748	(12)	7.7	1.1
BT1C3	0.3260	(12)	0.0219	(39)	0.1976	(18)	6.4	1.4

Table 2. (Continued)

Atom	X/a	Error	Y/b	Error	Z/c	Error	B	Error
BT103	0.3414	(8)	0.0222	(26)	0.2402	(12)	7.2	1.0
BT2C1	0.2629	(13)	0.1294	(40)	0.0437	(19)	5.9	1.5
BT201	0.2773	(8)	0.1556	(26)	0.0079	(13)	7.5	1.0
BT2C2	0.1982	(17)	0.1539	(47)	0.0709	(21)	8.9	1.8
BT202	0.1704	(12)	0.1919	(36)	0.0504	(15)	12.3	1.4
BT2C3	0.2252	(14)	-0.0325	(57)	0.0784	(20)	8.3	1.8
BT203	0.2174	(9)	-0.1213	(33)	0.0569	(13)	9.0	1.1
BT3C1	0.2881	(13)	0.2537	(42)	0.2089	(16)	5.7	1.4
BT301	0.3142	(10)	0.3058	(32)	0.2224	(13)	9.4	1.2
BT3C2	0.2543	(12)	0.0846	(45)	0.2393	(20)	6.5	1.5
BT302	0.2545	(8)	0.0356	(31)	0.2765	(14)	9.4	1.2
BT3C3	0.2212	(15)	0.2577	(51)	0.2005	(19)	8.1	1.7
BT303	0.1993	(11)	0.3251	(35)	0.2174	(14)	11.3	1.3
BR1C1	0.3263	(12)	-0.0546	(38)	0.0250	(16)	5.6	1.4
BR1C2	0.2940	(12)	-0.0993	(42)	-0.0008	(19)	7.1	1.5
BR1C3	0.2896	(12)	-0.0760	(41)	-0.0542	(18)	5.8	1.4
BR1C4	0.3139	(14)	-0.0086	(44)	-0.0780	(18)	7.1	1.5
BR1C5	0.3430	(12)	0.0366	(40)	-0.0520	(18)	6.8	1.4
BR1C6	0.3508	(12)	0.0174	(42)	0.0017	(18)	7.3	1.5
BR2C1	0.3276	(10)	-0.2248	(39)	0.1048	(18)	4.8	1.3
BR2C2	0.3307	(11)	-0.2609	(43)	0.1550	(17)	5.5	1.3
BR2C3	0.3269	(12)	-0.3743	(50)	0.1657	(19)	7.6	1.6
BR2C4	0.3230	(12)	-0.4487	(43)	0.1276	(21)	7.4	1.6
BR2C5	0.3233	(12)	-0.4148	(45)	0.0767	(18)	6.5	1.4
BR2C6	0.3272	(13)	-0.2963	(51)	0.0634	(20)	8.7	1.7
BR3C1	0.3814	(11)	-0.0573	(38)	0.1075	(15)	4.6	1.3
BR3C2	0.4038	(14)	-0.1415	(43)	0.0859	(18)	7.3	1.6

Table 2. (Continued)

Atom	X/a	Error	Y/b	Error	Z/c	Error	B	Error
BR3C3	0.4429	(14)	-0.1206	(45)	0.0928	(19)	8.0	1.6
BR3C4	0.4583	(12)	-0.0389	(42)	0.1232	(17)	5.7	1.4
BR3C5	0.4349	(14)	0.0298	(42)	0.1469	(17)	6.9	1.5
BR3C6	0.3970	(12)	0.0268	(39)	0.1403	(16)	5.8	1.4
AR1C1	0.4992	(10)	0.5716	(35)	0.3720	(15)	4.2	1.2
AR1C2	0.5184	(12)	0.5548	(36)	0.3305	(16)	5.2	1.3
AR1C3	0.5559	(12)	0.5554	(38)	0.3318	(16)	6.4	1.4
AR1C4	0.5742	(11)	0.5714	(39)	0.3782	(17)	5.9	1.4
AR1C5	0.5579	(12)	0.5842	(38)	0.4227	(16)	5.5	1.3
AR1C6	0.5187	(12)	0.5899	(38)	0.4186	(15)	5.3	1.3
AR2C1	0.4429	(10)	0.6573	(40)	0.4261	(16)	4.3	1.3
AR2C2	0.4489	(11)	0.7718	(45)	0.4232	(17)	6.0	1.4
AR2C3	0.4425	(13)	0.8326	(45)	0.4704	(22)	8.8	1.7
AR2C4	0.4305	(13)	0.7855	(50)	0.5139	(19)	7.2	1.5
AR2C5	0.4266	(13)	0.6769	(51)	0.5147	(20)	8.3	1.6
AR2C6	0.4297	(12)	0.6089	(41)	0.4716	(19)	6.7	1.5
AR3C1	0.4376	(11)	0.6814	(33)	0.3202	(14)	3.2	1.1
AR3C2	0.4005	(11)	0.6899	(35)	0.3124	(15)	4.3	1.2
AR3C3	0.3885	(12)	0.7745	(40)	0.2733	(17)	5.9	1.4
AR3C4	0.4124	(14)	0.8269	(41)	0.2453	(18)	7.1	1.5
AR3C5	0.4496	(12)	0.8102	(38)	0.2540	(16)	5.6	1.4
AR3C6	0.4620	(11)	0.7362	(39)	0.2943	(16)	5.3	1.3

rigid groups. This refinement resulted in an R = 0.082 and wR = 0.097 with the heavy atoms again anisotropic. The calculated and observed structure factors based on this refinement are given in Figure 2. A final difference map was calculated and no peaks above 0.7 e/A^3 were found.

The final atomic parameters and their standard deviations computed from the least squares matrix are given in Figure 3. The important bond lengths are shown in Figure 4. The important interatomic distances and angles and their calculated standard errors are shown in Figures 5 and 6. Because of the comparatively small number of observations per variable, these results could conceivably be viewed with some distrust. A check on the accuracy of our results is afforded by the positional parameters of the benzene rings which resulted from our first series of refinements. The refined parameters were used to calculate 36 bond distances which were known to be equivalent, thereby giving a very reliable estimate of the errors in this structure determination. The average carbon-carbon bond distance was found to be 1.406 ± 0.007 Å in good agreement with the accepted value, indicating no serious systematic errors in this determination. The standard deviation of an individual measurement of a carbon-carbon bond length as calculated from the distribution of these distances is 0.043 Å. This can be compared to a typical

K= 0 L= 0			K= 0 L= 1			K= 0 L= 2			K= 0 L= 3			K= 0 L= 4		
H	OBS	CALC	H	OBS	CALC	H	OBS	CALC	H	OBS	CALC	H	OBS	CALC
2	365	220	0	138	125	18	411	440	2	198	196	2	198	196
4	616	465	4	141	108	20	57	37	4	127	109	4	127	109
6	694	621	12	159	153	-20	480	467	8	192	189	8	192	189
8	664	485	-12	163	153	-22	84	77	10	162	155	10	162	155
10	426	237				22	101	71	16	350	382	12	193	186
14	945	943	K= 0 L= 0			-24	187	196	-18	103	96	18	190	169
20	207	207	H	OBS	CALC	26	298	307	18	131	138			
22	224	226	5	180	189	-26	304	318	-20	49	27	K= 0 L= 4		
28	189	179	-5	197	189	28	249	215	20	76	59	H	OBS	CALC
30	186	174	11	127	105				-22	192	200	0	1144	1168
						K= 1 L= 2			24	227	229	4	324	217
K= 1 L= 0			K= 1 L= 1			H	OBS	CALC				6	226	199
H	OBS	CALC	H	OBS	CALC	1	815	786	K= 3 L= 3			8	273	290
1	198	166	1	339	337	3	200	166	H	OBS	CALC	-2	324	323
3	562	542	3	605	613	5	394	334	1	329	326	-4	473	486
5	168	176	5	357	337	9	187	210	3	209	171	-6	354	371
7	256	191	7	243	250	-1	691	729	5	204	204	-8	172	149
9	144	117	9	197	170	-5	357	360	7	187	201	10	207	233
11	202	237	-1	366	404	-7	230	192	9	123	98	-10	198	189
13	210	190	-3	430	453	-9	65	36	-1	461	480	12	205	189
15	264	179	-5	202	196	11	123	118	-5	89	67	-12	437	412
17	272	268	-7	143	126	-11	255	274	-7	367	385	-14	247	236
19	271	290	-9	271	268	-13	117	121	-9	129	116	-16	280	280
21	79	29	-11	421	401	13	317	316	-11	123	122	14	280	280
23	172	172	11	441	473	15	58	35	11	467	500	-16	37	55
27	182	186	13	66	16	-15	190	189	13	41	10	16	125	121
			-13	518	504	17	57	52	-13	37	29	-18	124	123
K= 2 L= 0			15	177	176	-17	68	83	15	224	257	18	153	148
H	OBS	CALC	-15	362	371	19	51	12	-15	471	498	-20	124	111
0	127	118	-17	48	36	-19	134	144	-17	36	22	22	136	132
2	362	345	17	406	450	21	52	61	17	367	392	24	164	160
4	83	83	-19	84	65	-21	79	69	-19	129	139	26	240	244
6	265	209	19	99	92	-23	221	238	19	161	167	30	152	151
8	142	134	21	100	96	27	202	197	-21	149	139			
10	116	88	-21	146	151				-27	158	142	K= 1 L= 4		
12	77	34	23	182	194	K= 2 L= 2						H	OBS	CALC
14	495	517	-25	148	138	H	OBS	CALC	K= 4 L= 3			1	138	151
16	226	219	-27	286	282	0	212	203	H	OBS	CALC	3	195	200
18	64	55	-29	159	143	2	237	207	2	420	410	5	101	72
20	69	81	29	190	183	4	237	224	4	542	531	7	190	197
28	230	219				6	213	181	6	148	142	9	71	36
			K= 2 L= 1			8	189	187	8	103	114	-1	280	222
K= 3 L= 0			H	OBS	CALC	-2	365	378	-2	261	279	-3	124	99
H	OBS	CALC	0	378	353	-4	210	187	-4	123	121	-5	163	165
5	335	370	2	202	182	-6	181	165	-6	229	237	-7	64	42
7	93	73	4	257	268	10	167	146	-8	313	325	-9	304	307
9	383	381	6	39	7	12	302	304	-10	147	134	11	156	162
11	73	16	8	147	156	-12	458	432	10	176	176	13	413	448
13	65	26	-2	261	299	-14	91	77	12	50	48	-13	422	436
15	125	124	-4	274	265	14	255	259	-12	273	314			
17	94	81	-8	242	241	-16	60	68	14	40	26	K= 5 L= 3		
19	42	24	10	93	81	16	108	112	-14	60	46	H	OBS	CALC
25	151	148	-10	153	164	-18	247	270	-16	77	76	1	37	11
			-12	107	91	18	303	327	-18	56	18	3	158	152
K= 4 L= 0			12	199	191	-20	61	13	18	66	46	5	144	139
H	OBS	CALC	14	124	146	20	167	159	20	220	221	7	26	42
0	202	164	-14	305	311	26	156	136				9	127	130
4	550	566	16	124	118	-28	178	182	K= 5 L= 3			-1	53	12
6	362	361	-16	344	318				H	OBS	CALC	-5	51	15
8	77	7	18	46	16	K= 3 L= 2			1	37	11	-7	121	116
10	371	380	-18	56	4	H	OBS	CALC	3	158	152	-9	273	292
12	172	187	20	148	167	1	124	135	5	144	139	11	73	85
14	196	203	-20	169	177	3	108	111	7	26	42	-11	105	100
16	171	165	-22	242	256	5	237	266	9	127	130	-13	135	146
18	75	77	-26	229	227	7	123	115	-1	53	12	13	303	339
						9	147	148	-5	51	15	-15	100	78
K= 5 L= 0			K= 5 L= 1			-3	246	283	-7	121	116	15	158	145
H	OBS	CALC	H	OBS	CALC	-5	172	164	-9	273	292	17	159	155
1	491	473	1	123	99	-7	112	123	11	73	85	-23	167	170
3	124	115	3	207	200	-9	221	240	-11	105	100			
5	207	213	5	90	93	-11	347	379	-13	135	146	K= 6 L= 3		
7	323	304	7	143	135	11	463	485	13	303	339	H	OBS	CALC
9	119	114	9	116	115	-13	117	92	-15	100	78	0	46	35
11	65	8	-1	259	274	13	147	138	15	158	145	2	77	59
13	125	114	-3	198	197	15	66	60	17	159	155	6	134	144
15	117	122	-5	183	171	-15	95	110	-23	167	170	8	187	171
21	142	140	-7	306	280	17	51	57				-4	39	34
			-9	66	15	-17	117	119	K= 6 L= 3			-6	98	115
K= 6 L= 0			11	109	88	-19	49	46	H	OBS	CALC	-8	83	82
H	OBS	CALC	-11	135	144	19	60	28	0	46	35	-10	160	169
2	494	518	13	30	8	-25	149	136	2	77	59	10	222	225
4	66	34	-13	81	91				6	134	144	-12	53	24
6	55	17	-15	130	154	K= 4 L= 2			8	187	171	12	116	111
8	66	71	17	63	29	H	OBS	CALC	-4	39	34			
10	91	16	-17	271	282	0	410	402	-6	98	115	K= 7 L= 3		
12	54	51	19	104	112	2	76	21	-8	83	82	H	OBS	CALC
16	205	212	-19	264	287	4	146	120	-10	160	169	1	184	198
-16	206	212	21	199	213	6	312	311	10	222	225	3	51	18
20	215	224	-23	166	149	8	75	61	-12	53	24	5	123	131
-20	206	224	25	196	192	-2	149	154	12	116	111	7	76	64
						-4	67	9				9	153	155
K= 7 L= 0			K= 7 L= 1			-6	190	205	K= 7 L= 3			11	129	126
H	OBS	CALC	H	OBS	CALC	-8	96	106	H	OBS	CALC	-11	335	361
1	66	42	2	310	271	-10	92	81	1	184	198			
3	166	166	4	230	201	10	199	207	3	51	18			
5	130	126	6	398	417	12	133	130	5	123	131			
7	115	120	8	119	116	-12	337	350	-1	179	193			
9	116	113	-2	215	209	14	72	46	-3	41	36			
13	166	165	-4	626	665	-14	78	91	-5	57	29			
-13	176	183	-6	112	109	-16	106	105	-7	194	230			
15	161	155	-8	374	392	16	221	248	13	139	121			
19	177	171	10	65	74	18	44	8	17	177	156			
-19	189	171	-10	143	150	-18	151	153						

K= 8 L= 3			K= 3 L= 4			K= 4 L= 4		
H	OBS	CALC	H	OBS	CALC	H	OBS	CALC
2	198	196	-13	68	27	0	201	192
4	127	109	13	209	219	4	171	127
8	192	189	-15	60	60	6	119	119
10	162	155	15	185	213	8	109	89
12	193	186	-17	118	120	-2	119	114
18	190	169	17	155	154	-4	155	152
			-19	49	37	-6	205	213
K= 9 L= 3			19	86	94	-8	125	119
H	OBS	CALC	-25	195	191	10	56	37
7	125	113	-27	187	179	-10	293	304
9	262	250				-12	221	230
-5	262	253	K= 4 L= 4			12	284	313
-9	235	243	H	OBS	CALC	-14	96	97
			0	201	192	14	235	273
K= 0 L= 4			4	171	127	16	63	30
H	OBS	CALC	6	119	119	-16	263	268
0	1144	1168	8	109	89	-18	114	101
4	324	217	-2	119	114	18	149	145
6	226	199	-4	155	152	20	147	141
8	273	290	-6	205	213			
-2	324	323	-8	125	119	K= 5 L= 4		
-4	473	486	10	56	37	H	OBS	CALC
-6	354	371	-10	293	304	1	339	348
-8	172	149	-12	221	230	3	256	295
10	207	233	12	284	313	5	120	114
-10	198	189	-14	96	97	7	293	315
12	205	189	14	235	273	9	216	230
-12	437	412	16	63	30	-1	64	17
-14	247	236	-16	263	268	-3	114	84
14	280	280	-18	114	101	-5	145	157
-16	37	55	18	149	145	-7	154	156
16	125	121	20	147	141	-9	62	33
-18	124	123				11	54	32
18	153	148	K= 5 L= 4			-11	207	222
-20	124	111	H	OBS	CALC	-13	32	26
22	136	132	1	339	348	13	97	108
-22	164	160	3	256	295	15	79	88
26	240	244	5	120	114	-15	137	144
30	152	151	7	293	315	17	95	80
			9	216	230	19	128	126
K= 1 L= 4			-1	64	17	23	133	123
H	OBS	CALC	-3	114	84			
1	138	151	-5	145	157	K= 6 L= 4		
3	195	200	-7	154	156	H	OBS	CALC
5	101	72	-9	62	33	0	447	476
7	190	197	11	54	32	6	113	129
9	71	36	-11	207	222			
-1	280	222	-13	32	26	8	276	256
-3	124	99	13	97	108	-2	274	304
-5	163	165	15	79	88	-4	50	42
-7	64	42	-15	137	144	-6	59	8
-9	304	307	17	95	80	-8	59	50
11	156	162	19	128	126	10	78	85
-11	185	167	23	133	123	-10	256	264
13	413	448				-12	176	189
-13	422	436	K= 6 L= 4			20	150	129
15	50	24	H	OBS	CALC			
-15	82	70	0	447	476	K= 7 L= 4		
17	64	42	6	113	129	H	OBS	CALC
-17	275	308	8	276	256	1	259	273
19	59	62	-2	274	304	3	135	163
-19	291	282	-4	50	42	5	97	85
21	65	51	-6	59	8	7	199	206
-21	139	134	-8	59	50	-1	108	100
-31	181	187	10	78	85	-3	222	246
			-10	256	264	13	144	150
K= 2 L= 4			-12	176	189	-15	195	206
H	OBS	CALC	20	150	129			
0	261	202				K= 9 L= 4		
2	184	155	K= 7 L= 4			H	OBS	CALC
4	163	163	H	OBS	CALC	5	135	111
6	251	246	1	259	273			
8	328	336	3	135	163	K= 1 L= 5		
-2	230	219	5	97	85	H	OBS	CALC
-6	422	441	7	199	206	1	628	619
-8	352	351	-1	108	100	3	198	179
-10	266	254	-3	222	246	5	54	20
10	524	521	13	144	150	9	333	319
-12	101	95	-15	195	206	-1	180	152
12	107	93				-3	190	165
-14	298	309				-5	162	160
14	342	363				-9	68	12
-16	160	163				-11	101	83
16	186	205				11	116	92
18	36	51				-13	115	127
-18	127	132				13	134	132
-20	40	52				-15	128	130
20	48	42				17	53	9
						-17	86	81
K= 3 L= 4						19	43	11
H	OBS	CALC				-19	65	69
-1	180	152						
-3	190	165						
-5	162	160						
-9	68	12						
-11	101	83						
11	116	92						
-13	115	127						
13	134	132						
-15	128	130						
17	53	9						
-17	86	81						
19	43	11						
-19	65	69						

Figure 2. Calculated and observed structure factors

K= 1 L= 5		
H	OBS	CALC
23	174	185
-27	165	187
29	164	152

K= 2 L= 5		
H	OBS	CALC
0	222	182
2	68	47
4	152	151
6	220	231
8	106	111
-2	50	25
-4	84	58
-6	44	19
-8	105	94
-10	157	159
10	316	313
-12	90	60
12	428	418
14	63	15
-14	221	240
16	301	331
-16	293	314
-18	106	93
20	126	139
-20	275	286
22	201	182
-26	248	227

K= 3 L= 5		
H	OBS	CALC
1	455	473
3	50	14
5	660	695
7	126	129
9	223	231
-1	241	246
-3	430	455
-5	62	16
-7	238	240
-9	114	111
11	207	212
-11	541	593
13	284	307
-13	298	302
-15	266	289
15	402	450
17	47	50
-17	48	49
-19	193	196
-21	140	129
23	131	127

K= 4 L= 5		
H	OBS	CALC
0	102	93
4	61	30
6	636	653
8	37	48
-2	74	55
-4	61	35
-6	393	465
-8	239	258
10	35	16
-10	116	100
-12	179	229
12	216	250
14	61	82
-14	69	11
16	165	167
-16	194	194
-18	126	136

K= 5 L= 5		
H	OBS	CALC
1	144	158
3	111	138
5	62	52
7	75	95
9	36	33
-1	102	116
-5	216	259
-7	157	225
-9	22	11
-11	50	32
11	71	47
13	97	101
-13	104	126
-15	102	98
17	224	224
-19	135	144
21	190	196
23	135	133

K= 6 L= 5		
H	OBS	CALC
0	235	208
2	165	186
3	142	137
8	42	45
-2	105	101
-4	91	107
-8	46	49

K= 6 L= 5		
H	OBS	CALC
-10	116	138
10	143	153
16	130	133
20	146	179

K= 7 L= 5		
H	OBS	CALC
3	233	234
3	234	234
5	181	179
7	176	167
9	136	137
-1	196	203
-19	182	180

K= 8 L= 5		
H	OBS	CALC
0	167	175
4	146	154
-14	152	138
16	144	144
18	185	196

K= 9 L= 5		
H	OBS	CALC
5	229	203
13	197	205

K= 0 L= 6		
H	OBS	CALC
2	193	183
4	280	286
6	472	432
8	306	294
-2	369	368
-4	155	162
-6	72	34
10	108	136
-10	404	392
-12	158	148
12	188	172
-14	140	135
14	268	276
-16	89	80
-18	318	333
-20	268	284
-22	135	148
22	151	153
-28	155	155
28	263	277
-30	105	77

K= 1 L= 6		
H	OBS	CALC
1	203	199
3	233	244
5	112	82
7	341	360
9	521	530
-1	125	133
-3	130	102
-5	279	291
-7	111	97
-9	251	230
11	304	313
13	127	124
-13	205	215
-15	56	46
15	111	122
17	39	11
-17	100	105
19	48	7
-19	70	66
-21	215	223
-23	215	205
27	170	179

K= 2 L= 6		
H	OBS	CALC
0	183	192
2	45	23
4	45	21
6	80	53
8	293	316
-4	204	207
-6	150	143
-8	352	365
10	96	76
-10	432	457
-12	113	111
12	259	257
-14	99	93
14	286	309
16	65	76
-16	136	153
18	109	103
-18	130	111
-20	46	21
20	137	133
24	158	158
-24	130	163
-28	200	191

K= 3 L= 6		
H	OBS	CALC
1	83	91
3	159	135
5	548	518
7	160	158
9	167	168
-1	330	326
-5	135	134
-7	94	106
-9	125	107
11	96	80
-11	97	87
13	76	71
-13	74	62
-15	72	80
15	180	198
17	126	142
-17	132	141
-19	93	90
19	214	234
21	230	226
23	151	149

K= 4 L= 6		
H	OBS	CALC
0	326	361
2	78	51
4	254	260
6	152	146
8	166	175
-2	117	96
-6	98	92
-8	304	339
-10	70	64
10	143	150
12	66	58
-12	230	266
14	118	127
-14	151	167
-16	102	74
16	128	109
18	156	143

K= 5 L= 6		
H	OBS	CALC
1	142	158
5	49	17
7	89	94
9	92	82
-1	69	64
-3	255	280
-5	259	293
-7	39	115
-9	74	61
-13	90	107
13	55	94

K= 6 L= 6		
H	OBS	CALC
2	368	389
4	80	52
6	294	288
8	162	169
-2	69	72
-4	266	296
-6	113	122
-8	146	159
-10	136	120
-14	160	165

K= 7 L= 6		
H	OBS	CALC
1	204	189
5	203	204
11	155	154

K= 8 L= 6		
H	OBS	CALC
0	191	182
-6	183	161

K= 1 L= 7		
H	OBS	CALC
1	362	355
3	74	65
5	59	51
7	181	153
9	96	89
-1	227	224
-3	75	14
-5	49	23
-7	59	13
-9	205	189
11	75	43
-11	126	109
-13	170	169
13	187	210
-15	84	33
15	129	150
17	39	3
-17	72	86
-19	79	89
19	86	94
23	136	131

K= 1 L= 7		
H	OBS	CALC
25	124	101
-25	149	190
27	117	110

K= 2 L= 7		
H	OBS	CALC
0	283	249
2	52	7
4	104	90
6	127	119
8	99	75
-2	133	99
-4	133	134
-6	56	36
-8	169	171
-10	186	180
10	202	214
-12	66	17
12	100	89
-14	88	91
14	217	241
16	140	153
-16	223	246
-18	168	176
18	185	189
-22	200	189
24	236	227

K= 3 L= 7		
H	OBS	CALC
1	248	213
3	155	151
5	86	84
7	382	405
9	146	166
-1	385	398
-3	243	238
-5	190	187
-7	346	367
-9	195	184
-11	331	388
11	546	597
-13	51	45
13	79	68
15	45	13
-15	300	296
-17	245	279
17	342	371
-19	144	133
19	159	143
-27	197	195

K= 4 L= 7		
H	OBS	CALC
0	271	279
4	284	295
6	203	201
8	66	52
-2	313	345
-4	142	135
-6	251	271
-8	291	330
-10	72	57
10	237	266
-12	105	98
12	224	236
14	75	55
-14	201	227
-16	78	60
16	191	208
20	144	148
24	212	196

K= 5 L= 7		
H	OBS	CALC
3	195	233
5	117	117
7	152	156
9	68	39
-1	79	56
-3	288	326
-5	134	148
-7	145	141
-9	158	163
11	59	59
-13	151	136
-17	250	256
21	222	231
-21	242	232

K= 6 L= 7		
H	OBS	CALC
0	182	167
4	131	121
-2	111	121
-4	50	45
-6	127	119
-8	64	63
-14	210	203
-16	227	224

K= 7 L= 7		
H	OBS	CALC
1	261	263
5	166	177
-1	151	135
17	122	102

K= 8 L= 7		
H	OBS	CALC
2	154	157
4	202	189
10	149	137
12	154	149

K= 9 L= 7		
H	OBS	CALC
1	173	144
7	197	211
9	210	208
-7	218	230
-9	195	200

K= 0 L= 8		
H	OBS	CALC
0	281	254
2	66	57
4	401	398
6	146	149
8	377	370
-2	669	707
-4	105	107
-6	343	335
-8	101	69
-10	251	257
10	516	526
-12	175	157
12	309	326
-14	251	275
-16	144	147
18	138	156
-18	148	148
20	164	167
-20	159	157
22	175	180
-22	176	144
-24	157	159
26	393	430

K= 1 L= 8		
H	OBS	CALC
1	93	53
5	338	329
7	187	194
9	178	177
-1	76	47
-3	126	123
-5	107	98
-7	205	218
-9	317	324
11	67	75
-11	68	66
-13	50	35
13	282	316
-15	83	84
15	103	97
17	169	192
-17	339	350
-19	271	292
23	160	174

K= 2 L= 8		
H	OBS	CALC
0	173	157
2	59	52
4	141	136
6	91	83
8	168	141
-2	393	384
-4	117	118
-6	195	213
-8	66	13
10	146	156
-10	191	214
-12	112	109
12	270	262
14	92	76
-14	129	122
16	77	63
-16	221	232
-18	63	55
-20	205	196
-22	197	194
-24	191	193

K= 3 L= 8		
H	OBS	CALC
3	138	138
5	103	85
7	105	108
9	79	71
-1	101	85
-7	62	25
-9	254	290
11	63	49
-11	139	145

K= 3 L= 8		
H	OBS	CALC
13	37	6
15	23	29
-15	68	54
-17	69	67
17	142	138
19	148	143
21	158	153

K= 4 L= 8		
H	OBS	CALC
0	276	290
4	174	186
6	28	24
8	71	40
-2	66	44
-4	98	77
-6	44	16
-8	166	183
-10	77	76
10	210	220
12	124	122
14	318	344
16	147	142
-16	267	256
20	214	220
22	165	158

K= 5 L= 8		
H	OBS	CALC
1	323	357
3	381	409
5	75	72
7	84	97
9	43	7
-1	126	127
-3	309	326
-5	187	199
-7	162	160
-9	129	127
11	67	39
-11	118	126
-13	65	57
-15	168	143
-17	134	134

K= 6 L= 8		
H	OBS	CALC
0	270	301
2	111	116
6	238	257
-2	231	274
-4	173	196
-6	63	56
-10	227	247
-12	179	192
-14	186	184
-16	227	216
-22	175	171

K= 7 L= 8		
H	OBS	CALC
1	220	216
7	197	206
-5	152	164
13	178	199
17	147	130

K= 8 L= 8		
H	OBS	CALC
-8	160	158
10	146	133

K= 1 L= 9		
H	OBS	CALC
1	157	146
3	57	36
5	75	70
7	146	142
9	88	94
-1	753	756
-3	95	15
-7	149	162
-9	78	63
11	79	83
-11	149	166
-13	39	24
13	177	172
15	179	196
-15	196	193
17	41	32
-17	179	169
-19	81	20
23	187	172
-29	134	150

K= 2 L= 9		
H	OBS	CALC
0	140	134
2	100	95
4	269	241
6	278	283
8	48	52
-2	113	105

K= 2 L= 9		
H	OBS	CALC
-4	222	208
-8	120	117
-10	159	166
10	239	241
-12	70	79
12	274	295
14	92	81
16	148	159
-18	145	155
18	286	297
-20	250	250
-26	180	162

K= 3 L= 9		
H	OBS	CALC
1	56	55
3	50	31
5	149	129
9	135	142
-1	310	290
-3	413	417
-5	245	242
-7	184	206
-9	128	132
11	201	203
-13	229	265
13	362	388
15	115	124
-15	223	235
-17	104	96
-19	152	153
19	176	180
-21	136	142
23	220	236
-25	187	200

K= 4 L= 9		
H	OBS	CALC
0	177	175
2	136	124
6	138	153
8	30	11
-2	207	214
-8	73	71
10	81	74
-10	149	142
-12	87	101
12	108	111
-16	157	151
-20	129	127
20	277	270

K= 5 L= 9		
H	OBS	CALC
1	226	255
7	50	50
9	81	66
-1	193	197
-3	118	129
-5	110	128
-7	90	104
-9	50	43
-17	159	171
23	125	143

K= 6 L= 9		
H	OBS	CALC
0	159	169
2	207	183
8	136	130
-2	47	20
-6	146	132
10	151	145
-10	155	156

K= 7 L= 9		
H	OBS	CALC
3	158	159
-1	275	300
15	166	167
-15	298	320
-19	210	203

K= 8 L= 9		
H	OBS	CALC
4	156	160
8	133	122

K= 9 L= 9		
H	OBS	CALC
5	185	165

K= 0 L=10		
H	OBS	CALC
0	407	367
4	180	194
-2	463	430
-4	622	629
-8	369	416
-10	258	282
10	347	416
-12	199	221
12	250	244

K= 0 L=10		
H	OBS	CALC
14	92	92
-14	97	105
-16	118	105
16	205	231
-18	100	103
-20	112	92
22	177	169

K= 1 L=10		
H	OBS	CALC
3	360	374
7	360	386
9	376	435
-1	79	75
-3	217	222
-7	153	151
-9	191	198
-11	71	52
11	121	125
-13	123	127
-15	42	33
15	81	85
-21	201	182
21	216	216
23	165	163
-23	256	258

K= 2 L=10		
H	OBS	CALC
2	240	240
4	379	376
6	94	101
8	129	136
-2	181	199
-4	106	86
-6	130	129
-8	164	162
-10	134	126
12	102	118
-12	104	107
14	279	306
-14	289	313
-16	99	92
16	138	138
-18	191	179
20	137	142
24	188	185

K= 3 L=10		
H	OBS	CALC
1	173	173
3	85	58
7	28	17
9	82	60
-1	242	254
-3	120	120
-5	383	439
-7	141	134
-9	44	44
-11	40	42
11	72	67
13	46	23
-13	58	60
-15	70	89
15	224	214
17	171	179
-21	118	113
21	249	253
-25	134	129

K= 4 L=10		
H	OBS	CALC
0	313	350
2	218	192
6	97	100
8	54	72
-2	93	74
-4	42	14
-6	54	30
-8	94	69
-10	124	142
10	178	179
14	168	159
-14	243	245
-20	162	147

K= 5 L=10		
H	OBS	CALC
1	272	287
5	62	37
7	107	109
-1	122	115
-3	153	155
-5	354	401
-7	142	144
-9	33	10
-11	248	252
-15	140	140
-17	213	221
19	129	142
-19	191	180

Figure 2. (Continued)

K 6 L 10

H	OBS	CALC
0	156	141
2	325	350
4	246	264
8	114	117
-6	267	294
10	168	165

K 7 L 10

H	OBS	CALC
5	230	210
9	208	222
-9	188	189
-13	158	158

K 1 L 11

H	OBS	CALC
1	250	246
5	201	205
7	203	197
9	267	291
-1	93	81
-3	53	13
-5	365	401
-7	273	298
-9	57	28
11	80	61
-11	86	72
13	70	62
-13	253	261
-15	135	128
-17	98	102
-19	145	138
23	154	152
-27	192	178

K 2 L 11

H	OBS	CALC
0	81	81
2	178	175
4	67	68
8	110	115
-2	153	149
-4	152	150
-6	210	230
-8	245	270
-10	43	18
10	182	193
12	93	99
-12	151	151
-14	57	32
14	186	194
-16	90	101
-18	180	180
20	131	115
-22	154	152
24	170	159
-24	231	243

K 3 L 11

H	OBS	CALC
3	190	181
5	89	120
7	274	270
9	137	131
-1	82	52
-3	120	93
-7	119	141
-9	50	54
-11	88	82
11	186	196
-13	110	111
13	137	114
15	235	244
-17	166	163
17	249	266
-21	148	129
21	169	168
-25	174	176

K 4 L 11

H	OBS	CALC
0	60	28
2	211	209
4	194	216
8	134	139
-2	182	190
-4	111	-26
-8	199	209
-10	124	138
10	125	116
14	127	130

K 5 L 11

H	OBS	CALC
3	108	95
5	95	83
-1	231	253
-3	242	255
-7	119	127
21	154	166
-21	223	216

K 6 L 11

H	OBS	CALC
0	169	158
-4	168	154
10	212	204
-14	194	205
16	149	151

K 7 L 11

H	OBS	CALC
3	144	141
7	135	124
-7	176	181
-15	174	174

K 8 L 11

H	OBS	CALC
8	136	122

K 0 L 12

H	OBS	CALC
0	177	121
2	80	93
4	133	168
6	109	102
8	228	250
-2	611	672
-4	252	268
-6	63	42
-8	65	44
10	89	89
-10	147	132
-12	99	127
14	127	127
-14	185	192
-16	182	185
-18	115	100
-22	193	201
22	212	214
24	169	169

K 1 L 12

H	OBS	CALC
1	162	151
5	170	184
7	132	135
9	92	100
-3	139	132
-5	82	112
-7	107	96
-9	285	317
11	50	32
-11	191	179
-13	193	207
13	359	393
15	160	169
-15	203	195
17	152	160
19	151	135
23	166	169
-27	155	159

K 2 L 12

H	OBS	CALC
2	201	217
4	142	139
8	142	143
-4	62	32
-6	241	264
-8	62	18
-10	93	99
-12	35	22
12	180	171
-16	120	129
-18	160	149
-22	139	135
24	142	135
-24	198	192

K 3 L 12

H	OBS	CALC
1	357	371
5	103	79
7	112	112
9	63	70
-1	186	170
-3	104	71
-9	71	63
-11	35	15
21	166	164
-21	164	154

K 4 L 12

H	OBS	CALC
2	123	110
4	65	49
-4	249	261
-6	138	168
-8	164	179
10	155	165
14	163	158
16	153	146
-16	222	215

K 5 L 12

H	OBS	CALC
3	160	148
5	141	123
-3	156	152
-7	161	156
-9	125	131
15	152	159

K 6 L 12

H	OBS	CALC
6	189	197
8	183	185
-2	324	352
-4	198	195
-18	152	172

K 7 L 12

H	OBS	CALC
1	220	234
11	135	134

K 1 L 13

H	OBS	CALC
9	67	63
-1	411	459
-3	99	110
-5	128	122
-7	161	180
-9	122	117
11	21	37
-11	68	64
-13	171	178
13	204	203
-15	180	168
-19	154	136

K 2 L 13

H	OBS	CALC
2	122	117
4	86	73
6	222	245
-4	140	150
-6	138	138
-8	162	175
10	45	34
-12	68	67
12	159	171
14	151	155

K 3 L 13

H	OBS	CALC
1	122	139
3	252	269
7	213	207
-3	183	187
-5	99	83
-7	153	153
-9	22	38
11	174	181
-13	160	159
13	342	349
-17	142	141
19	217	224
-21	161	150

K 4 L 13

H	OBS	CALC
0	101	105
2	81	103
4	139	127
6	190	193
-2	196	199
-4	47	18
-6	154	159
-12	129	143
14	156	144
20	107	107
-20	118	105

K 5 L 13

H	OBS	CALC
1	152	147
7	148	146
-5	158	159
-17	171	149
-21	160	176

K 0 L 14

H	OBS	CALC
0	352	356
2	293	334
6	153	153
8	106	125
-2	168	193
-4	125	150
-6	97	82
-8	428	454
10	175	160
-10	447	511
-12	251	256
12	356	375
14	189	172
-16	253	238
18	168	169
20	139	147
-22	132	129

K 1 L 14

H	OBS	CALC
1	92	73
3	191	204
7	104	105
9	234	243
-1	135	120
-5	212	194
-9	125	130
-11	81	69
13	150	151
-13	173	186
17	123	123
19	136	144
-23	106	100

K 2 L 14

H	OBS	CALC
2	153	160
6	142	149
-2	225	232
-4	53	33
-6	100	106
-10	63	26
-12	127	125
14	165	166
-14	160	160
16	140	136
-16	155	159
18	147	149
-22	136	125

K 3 L 14

H	OBS	CALC
1	173	178
7	120	115
-3	65	15
-5	211	221
-7	101	66

K 4 L 14

H	OBS	CALC
2	120	110
12	177	172
-14	213	224

K 5 L 14

H	OBS	CALC
5	143	147
-1	235	236
-3	159	165
-7	212	218
13	146	140

K 6 L 14

H	OBS	CALC
0	189	197
2	209	225
-6	199	193
10	149	154

K 7 L 14

H	OBS	CALC
9	153	136
-3	187	185

K 1 L 15

H	OBS	CALC
1	205	209
7	111	103
-1	198	205
-5	198	200
-13	121	125
-17	142	134

K 2 L 15

H	OBS	CALC
2	90	97
8	205	217
-2	127	127
-4	132	129
-8	141	135
10	157	154
-12	226	251
-14	141	138
14	179	173
18	114	116
-18	197	221

K 3 L 15

H	OBS	CALC
7	213	216
9	154	160
-7	173	169
11	141	128
-11	140	135
15	302	316
17	138	131
-17	157	154

K 4 L 15

H	OBS	CALC
2	265	286
4	205	210
8	132	122
-10	158	153
14	128	138
18	154	157

K 5 L 15

H	OBS	CALC
5	111	114
-1	205	201

K 6 L 15

H	OBS	CALC
-4	182	196
10	164	158

K 7 L 15

H	OBS	CALC
-1	127	135

K 0 L 16

H	OBS	CALC
4	136	116
-2	222	244
-4	399	376
-10	152	148
-14	273	269
16	227	225
18	119	113

K 1 L 16

H	OBS	CALC
1	72	70
5	150	131
-9	227	257
-13	179	188
-17	104	92
19	154	137

K 2 L 16

H	OBS	CALC
2	208	209
4	212	231
6	173	194
10	190	192
12	121	117
-12	206	221
16	137	117
-18	169	171

K 3 L 16

H	OBS	CALC
1	197	181
-5	129	145
-19	155	175

K 4 L 16

H	OBS	CALC
-4	163	161
-8	163	168
10	235	225

K 5 L 16

H	OBS	CALC
-3	190	187
-9	209	212

K 6 L 16

H	OBS	CALC
0	146	139
4	147	138
-2	264	260

K 7 L 16

H	OBS	CALC
1	171	171

K 1 L 17

H	OBS	CALC
3	174	181
-1	162	139
-3	202	207
-13	217	221
-19	162	148

K 2 L 17

H	OBS	CALC
6	132	112
14	210	206
16	211	224

K 3 L 17

H	OBS	CALC
3	218	223
7	192	186
-3	178	181
-5	186	176
11	214	217
13	177	206

K 4 L 17

H	OBS	CALC
2	188	178
6	165	169
8	183	188
-4	156	158
-6	144	140
-12	194	167

K 5 L 17

H	OBS	CALC
3	149	135

K 0 L 18

H	OBS	CALC
0	354	348
2	156	152
-2	264	270
-6	254	228
-8	279	266
10	142	127
14	237	240

K 1 L 18

H	OBS	CALC
3	201	211
-13	145	143

K 2 L 18

H	OBS	CALC
8	155	166
-2	274	271
12	151	163
-16	142	135

K 3 L 18

H	OBS	CALC
1	152	148
5	167	169
7	145	139

K 4 L 18

H	OBS	CALC
6	146	121
-4	150	150

K 5 L 18

H	OBS	CALC
-1	266	275
-7	298	290

K 1 L 19

H	OBS	CALC
-1	250	243
13	174	173
-15	155	160

K 2 L 19

H	OBS	CALC
2	223	228
8	190	198

K 3 L 19

H	OBS	CALC
7	181	184
-11	148	139

K 4 L 19

H	OBS	CALC
2	152	149

K 5 L 19

H	OBS	CALC
1	134	131

K 0 L 20

H	OBS	CALC
0	135	126
4	175	166
-2	219	210
-4	323	319
10	133	125

K 1 L 20

H	OBS	CALC
-1	324	327
-5	169	156

K 2 L 20

H	OBS	CALC
2	166	153

K 3 L 20

H	OBS	CALC
5	142	131

K 1 L 21

H	OBS	CALC
3	147	140
-3	203	190

K 2 L 21

H	OBS	CALC
4	152	140

K 0 L 22

H	OBS	CALC
0	264	282
-4	216	212

Figure 2. (Continued)

ATOM	x/a	y/b	z/c	β_{11}[a]	β_{22}	β_{33}	β_{12}	β_{13}	β_{23}
AFe1	0.3958(2)	0.2132(5)	0.3506(2)	8(1)	48(6)	17(1)	-1(2)	1(1)	-1(2)
AFe2	0.4235(2)	0.4164(5)	0.3617(2)	6(1)	50(7)	13(1)	2(2)	0(1)	-1(2)
AFe3	0.4665(2)	0.2527(5)	0.3595(2)	7(1)	52(7)	15(1)	-1(2)	-1(1)	1(2)
BFe1	0.2993(2)	0.0319(5)	0.1424(2)	6(1)	72(7)	16(1)	0(2)	-1(1)	-3(3)
BFe2	0.2362(2)	0.0979(6)	0.0944(2)	8(1)	100(8)	17(2)	8(2)	-3(1)	-5(3)
BFe3	0.2536(2)	0.1740(6)	0.1842(3)	8(1)	111(8)	19(2)	10(2)	-1(1)	-14(3)
AP	0.4507(3)	0.5789(9)	0.3705(4)	5(1)	46(13)	9(2)	1(3)	-0(1)	-3(4)
BP	0.3332(3)	-0.0769(10)	0.0957(4)	7(1)	72(14)	12(2)	2(3)	-1(1)	3(5)

ATOM	x/a	y/b	z/c	B	ATOM	x/a	y/b	z/c	B
AT1C1	0.399(1)	0.220(4)	0.284(2)	5.4(12)	AR1C1	0.500	0.573	0.373	3.4(10)
AT101	0.399(1)	0.218(2)	0.239(1)	5.6(7)	AR1C2	0.518	0.555	0.328	4.0(10)
AT1C2	0.398(1)	0.216(4)	0.417(2)	6.6(13)	AR1C3	0.556	0.555	0.331	5.6(12)
AT102	0.396(1)	0.225(3)	0.463(1)	7.8(9)	AR1C4	0.575	0.572	0.379	4.1(11)
AT1C3	0.395(1)	0.075(4)	0.351(2)	5.8(12)	AR1C5	0.557	0.590	0.423	3.7(10)
AT103	0.400(1)	-0.025(3)	0.354(1)	7.2(9)	AR1C6	0.519	0.591	0.420	3.8(10)
AT1C4	0.348(1)	0.227(4)	0.344(2)	6.4(13)	AR2C1	0.442	0.657	0.426	3.4(10)
AT104	0.319(1)	0.242(3)	0.344(1)	8.7(10)	AR2C2	0.448	0.769	0.425	5.7(12)
AT2C1	0.390(1)	0.443(3)	0.400(2)	4.6(11)	AR2C3	0.443	0.833	0.468	8.0(15)
AT201	0.364(1)	0.462(1)	0.426(1)	6.7(8)	AR2C4	0.431	0.784	0.513	5.6(12)
AT2C2	0.397(1)	0.449(4)	0.306(2)	4.9(11)	AR2C5	0.426	0.672	0.514	5.4(12)
AT202	0.379(1)	0.470(2)	0.268(1)	5.7(8)	AR2C6	0.431	0.608	0.471	5.8(13)
AT3C1	0.470(1)	0.155(4)	0.312(1)	6.2(13)	AR3C1	0.438	0.679	0.320	2.7(9)
AT301	0.471(1)	0.083(3)	0.282(1)	6.2(8)	AR3C2	0.401	0.696	0.311	3.8(10)
AT3C2	0.472(1)	0.164(4)	0.411(2)	4.6(11)	AR3C3	0.388	0.770	0.274	4.5(11)
AT302	0.476(1)	0.104(3)	0.447(1)	6.6(8)	AR3C4	0.412	0.829	0.246	5.1(11)
AT3C3	0.511(1)	0.287(3)	0.362(1)	3.4(10)	AR3C5	0.449	0.813	0.255	3.5(10)
AT303	0.543(1)	0.300(2)	0.363(1)	6.0(8)	AR3C6	0.462	0.738	0.292	4.3(11)
BT1C1	0.319(1)	0.150(4)	0.120(2)	5.1(12)	BR1C1	0.326	-0.056	0.026	3.2(10)
BT101	0.337(1)	0.212(3)	0.101(1)	5.9(8)	BR1C2	0.296	-0.098	-0.001	5.7(12)
BT1C2	0.272(1)	-0.071(4)	0.161(2)	4.3(11)	BR1C3	0.289	-0.076	-0.053	4.5(11)
BT102	0.256(1)	-0.147(3)	0.175(1)	5.4(8)	BR1C4	0.313	-0.009	-0.079	5.8(12)
BT1C3	0.326(1)	0.026(4)	0.197(2)	5.6(12)	BR1C5	0.343	0.035	-0.051	6.0(13)
BT103	0.342(1)	0.024(2)	0.240(1)	5.5(8)	BR1C6	0.350	0.013	0.001	5.5(12)
BT2C1	0.225(1)	-0.039(5)	0.075(2)	7.0(14)	BR2C1	0.329	-0.226	0.104	3.1(10)
BT201	0.216(1)	-0.123(3)	0.059(1)	7.9(9)	BR2C2	0.330	-0.260	0.156	4.4(11)
BT2C2	0.262(1)	0.129(4)	0.044(2)	5.2(11)	BR2C3	0.327	-0.371	0.167	5.9(13)
BT202	0.277(1)	0.157(2)	0.008(1)	6.0(8)	BR2C4	0.324	-0.448	0.127	6.3(13)
BT2C3	0.198(1)	0.149(4)	0.070(2)	7.3(14)	BR2C5	0.323	-0.413	0.076	5.3(12)
BT203	0.171(1)	0.194(3)	0.051(1)	9.3(11)	BR2C6	0.325	-0.302	0.065	5.5(12)
BT3C1	0.289(1)	0.252(4)	0.208(2)	4.5(11)	BR3C1	0.382	-0.061	0.108	3.3(10)
BT301	0.314(1)	0.308(3)	0.222(1)	7.7(9)	BR3C2	0.404	-0.135	0.084	5.6(12)
BT3C2	0.255(1)	0.089(4)	0.240(2)	4.8(12)	BR3C3	0.442	-0.126	0.092	5.4(12)
BT302	0.254(1)	0.034(3)	0.276(1)	8.0(9)	BR3C4	0.457	-0.042	0.123	4.2(11)
BT3C3	0.221(1)	0.258(4)	0.200(2)	6.8(14)	BR3C5	0.434	0.032	0.146	5.7(12)
BT303	0.200(1)	0.325(3)	0.217(1)	9.5(11)	BR3C6	0.397	0.023	0.139	5.0(11)

ABC1	0.453(1)	0.358(4)	0.415(2)	4.4(11)	BBC1	0.214(1)	0.071(4)	0.155(2)	4.9(11)
AB01	0.466(1)	0.376(2)	0.458(1)	5.2(7)	BB01	0.189(1)	0.024(3)	0.172(1)	6.7(8)
ABC2	0.455(1)	0.361(3)	0.309(2)	4.4(11)	BBC2	0.255(1)	0.248(4)	0.122(2)	4.4(11)
AB02	0.462(1)	0.382(2)	0.265(1)	4.0(7)	BB02	0.261(1)	0.338(3)	0.102(1)	6.3(8)

[a] β's are x10^4

Figure 3. Final atomic parameters from rigid body refinement

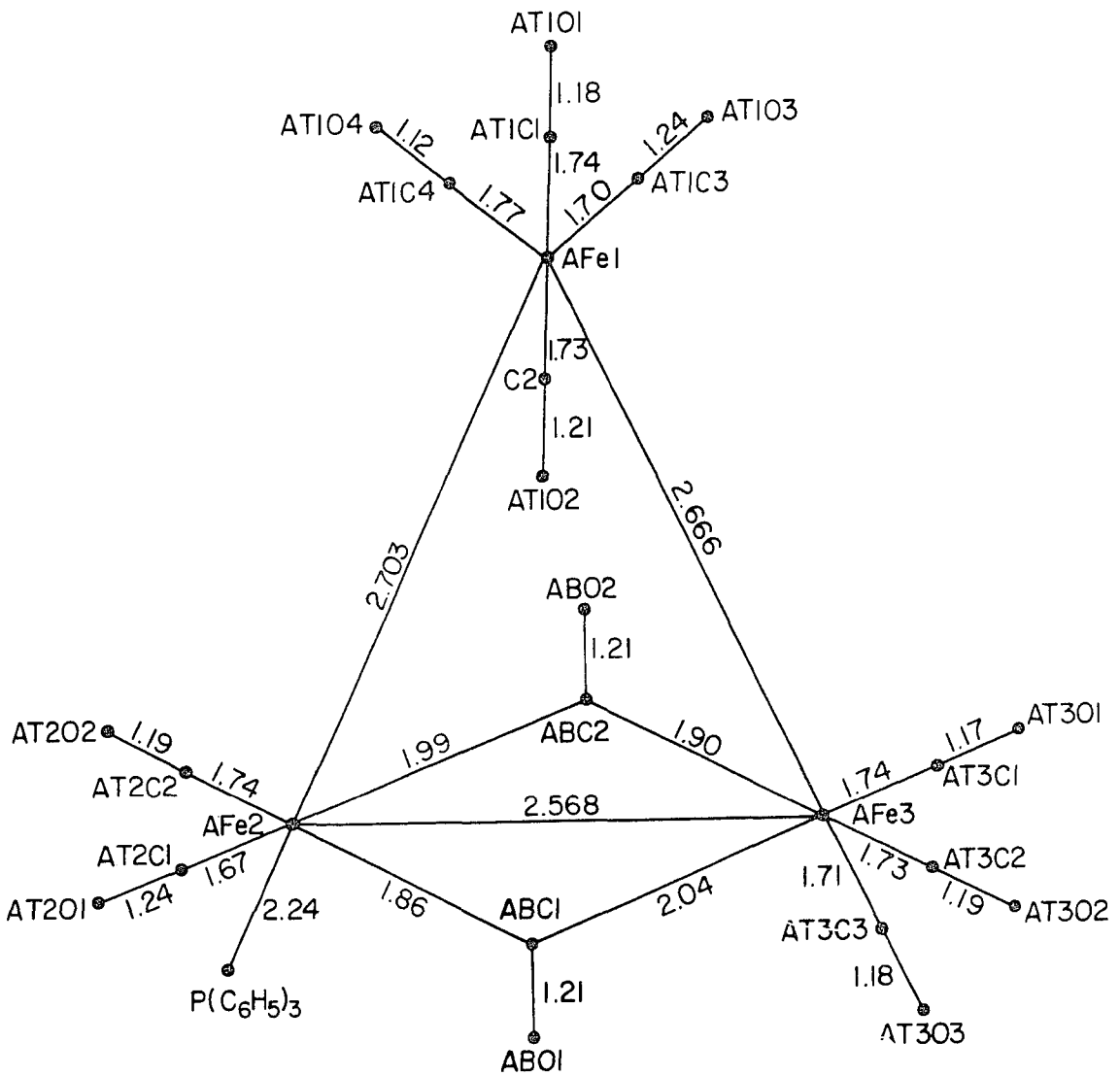

Figure 4. Sketch of two isomers of $Fe_3(CO)_{11}P(C_6H_5)_3$ showing important bond distances

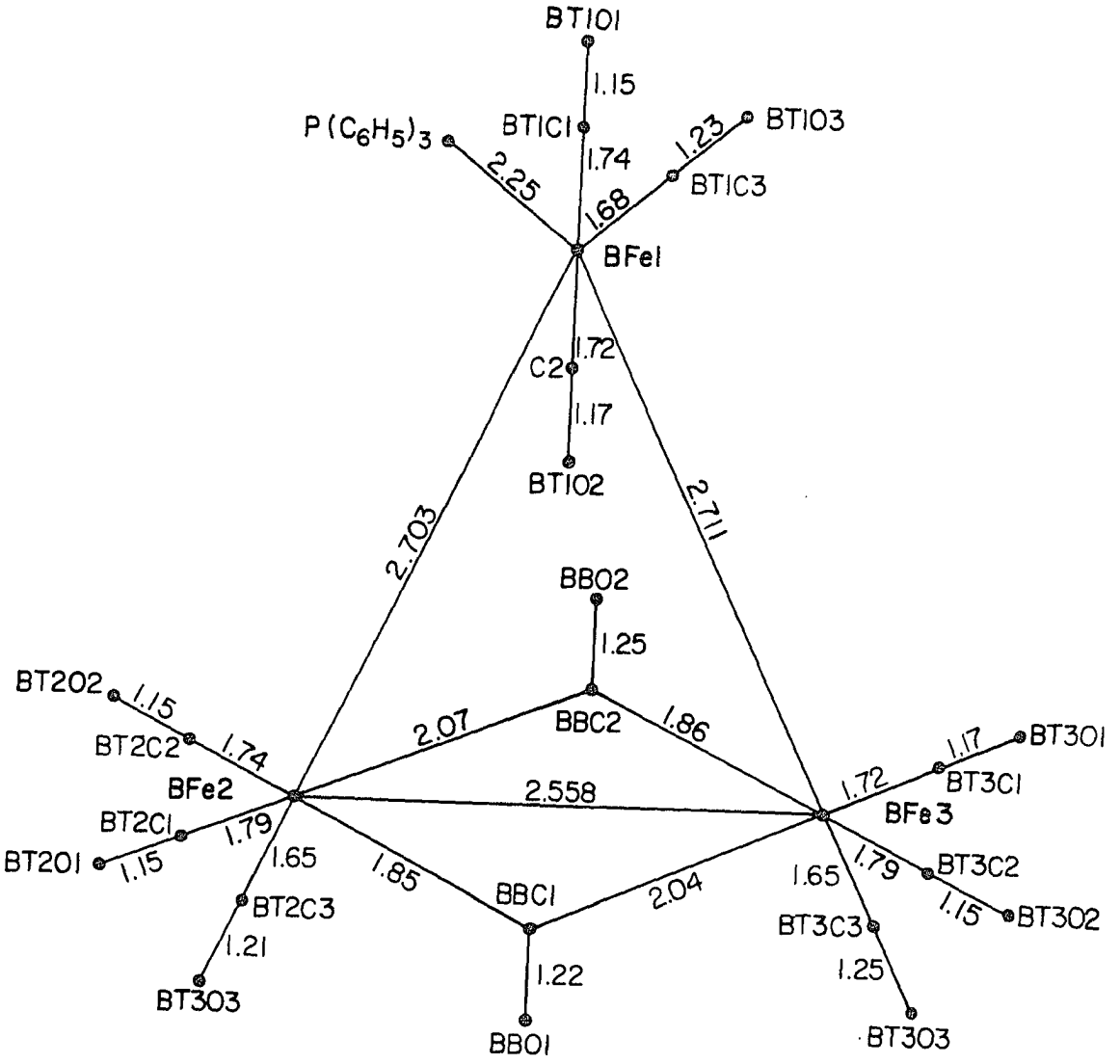

Figure 4. (Continued)

AFe1-AFe2	2.703(9)	AFe1-AT1C1	1.74(5)	AFe1-AT101	2.92(3)	AT1C1-AT101	1.18(4)
AFe1-AFe3	2.666(8)	AFe1-AT1C2	1.73(5)	AFe1-AT102	2.94(4)	AT1C2-AT102	1.21(5)
AFe2-AFe3	2.568(8)	AFe1-AT1C3	1.70(5)	AFe1-AT103	2.93(4)	AT1C3-AT103	1.24(5)
BFe1-BFe2	2.703(9)	AFe1-AT1C4	1.77(5)	AFe1-AT104	2.88(4)	AT1C4-AT104	1.12(5)
BFe1-BFe3	2.711(9)	AFe2-AT2C1	1.67(4)	AFe2-AT201	2.91(3)	AT2C1-AT201	1.24(4)
BFe2-BFe3	2.558(9)	AFe2-AT2C2	1.74(5)	AFe2-AT202	2.93(3)	AT2C2-AT202	1.19(4)
		AFe3-AT3C1	1.74(5)	AFe3-AT301	2.90(3)	AT3C1-AT301	1.17(5)
AFe2-AP	2.24(1)	AFe3-AT3C2	1.73(5)	AFe3-AT302	2.92(3)	AT3C2-AT302	1.19(4)
BFe1-BP	2.25(1)	AFe3-AT3C3	1.71(4)	AFe3-AT303	2.88(3)	AT3C3-AT303	1.18(4)
		BFe1-BT1C1	1.74(5)	BFe1-BT101	2.86(3)	BT1C1-BT101	1.15(4)
AFe2-ABC1	1.86(4)	BFe1-BT1C2	1.72(5)	BFe1-BT102	2.88(3)	BT1C2-BT102	1.17(4)
AFe2-ABC2	1.99(4)	BFe1-BT1C3	1.68(5)	BFe1-BT103	2.90(3)	BT1C3-BT103	1.23(4)
AFe3-ABC1	2.04(4)	BFe2-BT2C1	1.79(6)	BFe2-BT201	2.94(4)	BT2C1-BT201	1.15(5)
AFe3-ABC2	1.90(4)	BFe2-BT2C2	1.74(5)	BFe2-BT202	2.89(3)	BT2C2-BT202	1.16(4)
BFe2-BBC1	1.85(5)	BFe2-BT2C3	1.65(5)	BFe2-BT203	2.86(4)	BT2C3-BT203	1.21(5)
BFe2-BBC2	2.07(4)	BFe3-BT3C1	1.72(5)	BFe3-BT301	2.89(4)	BT3C1-BT301	1.18(4)
BFe3-BBC1	2.04(5)	BFe3-BT3C2	1.79(5)	BFe3-BT302	2.94(4)	BT3C2-BT302	1.15(4)
BFe3-BBC2	1.86(4)	BFe3-BT3C3	1.65(6)	BFe3-BT303	2.90(4)	BT3C3-BT303	1.25(5)
AFe2-AB01	2.93(3)	BFe2-BB01	2.91(3)	ABC1-AB01	1.21(4)	AP-	BP-
AFe2-AB02	3.01(3)	BFe2-BB02	3.09(3)	ABC2-AB02	1.21(4)	AR1C1 1.83	BR1C1 1.83
AFe3-AB01	2.99(3)	BFe3-BB01	3.04(3)	BBC1-BB01	1.22(4)	AR2C1 1.78	BR2C1 1.85
AFe3-AB02	2.93(3)	BFe3-BB02	2.96(3)	BBC2-BB02	1.25(4)	AR3C1 1.83	BR3C2 1.83

Figure 5. Atomic separations in Angstroms

AFe1-AFe2-AFe3	60.7(2)	AFe1-AT1C1-AT101	175(4)	AT1C1-AFe1-AT1C2	172(2)
AFe1-AFe3-AFe2	62.1(2)	AFe1-AT1C2-AT102	172(4)	AT1C1-AFe1-AT1C3	93(2)
AFe2-AFe1-AFe3	57.1(2)	AFe1-AT1C3-AT103	171(4)	AT1C1-AFe1-AT1C4	92(2)
BFe1-BFe2-BFe3	62.0(3)	AFe1-AT1C4-AT104	174(5)	AT1C2-AFe1-AT1C3	91(2)
BFe1-BFe3-BFe2	61.6(3)	AFe2-AT2C1-AT201	176(4)	AT1C2-AFe1-AT1C4	95(2)
BFe2-BFe1-BFe3	56.4(2)	AFe2-AT2C2-AT202	179(4)	AT1C3-AFe1-AT1C4	95(2)
		AFe3-AT3C1-AT301	175(4)	AT2C1-AFe2-AT2C2	93(2)
AFe2-ABC1-AFe3	82(2)	AFe3-AT3C2-AT302	179(4)	AT2C1-AFe2-ABC1	92(2)
AFe2-ABC2-AFe3	83(2)	AFe3-AT3C3-AT303	173(4)	AT2C1-AFe2-ABC2	167(2)
BFe2-BBC1-BFe3	82(2)	BFe1-BT1C1-BT101	166(4)	AT2C2-AFe2-ABC1	170(2)
BFe2-BBC2-BFe3	81(2)	BFe1-BT1C2-BT102	174(4)	AT2C2-AFe2-ABC2	80(2)
		BFe1-BT1C3-BT103	172(4)	ABC1-AFe2-ABC2	93(2)
AFe2-ABC1-AB01	144(4)	BFe2-BT2C1-BT201	173(5)	AT3C1-AFe3-AT3C2	96(2)
AFe2-ABC2-AB02	139(3)	BFe2-BT2C2-BT202	173(4)	AT3C1-AFe3-AT3C3	95(2)
AFe3-ABC1-AB01	132(3)	BFe2-BT2C3-BT203	175(5)	AT3C1-AFe3-ABC1	169(2)
AFe3-ABC2-AB02	139(3)	BFe3-BT3C1-BT301	177(4)	AT3C1-AFe3-ABC2	91(2)
BFe2-BBC1-BB01	142(4)	BFe3-BT3C2-BT302	177(4)	AT3C2-AFe3-AT3C3	94(2)
BFe2-BBC2-BB02	135(3)	BFe3-BT3C3-BT303	172(4)	AT3C2-AFe3-ABC1	82(2)
BFe3-BBC1-BB01	136(3)			AT3C2-AFe3-ABC2	171(2)
BFe3-BBC2-BB02	144(3)	AFe2-AP-AR1C1	115	AT3C3-AFe3-ABC1	96(2)
		AFe2-AP-AR2C1	117	AT3C3-AFe3-ABC2	91(2)
AP-AFe2-ABC1	91(1)	AFe2-AP-AR3C1	116	ABC1-AFe3-ABC2	90(2)
AP-AFe2-ABC2	95(1)	BFe1-BP-BR1C1	113	BT1C1-BFe1-BT1C2	169(2)
AP-AFe2-AT2C1	96(1)	BFe1-BP-BR2C1	117	BT1C1-BFe1-BT1C3	95(2)
AP-AFe2-AT2C2	96(1)	BFe1-BP-BR3C1	115	BT1C2-BFe1-BT1C3	93(2)
BP-BFe1-BT1C1	92(1)			BT2C1-BFe2-BT2C2	97(2)
BP-BFe1-BT1C2	95(1)	AFe1-AFe2-AT2C1	87(1)	BT2C1-BFe2-BT2C3	94(2)
BP-BFe1-BT1C3	96(2)	AFe1-AFe2-AT2C2	86(1)	BT2C1-BFe2-BBC1	88(2)
		AFe1-AFe3-AT3C1	86(1)	BT2C1-BFe2-BBC2	173(2)
AFe1-AFe2-AP	175.5(4)	AFe1-AFe3-AT3C2	91(1)	BT2C2-BFe2-BT2C3	98(2)
AFe3-AFe2-AP	114.8(4)	AFe1-AFe3-AT3C3	175(1)	BT2C2-BFe2-BBC1	171(2)
BFe2-BFe1-BP	115.3(4)	AFe2-AFe1-AT1C1	91(2)	BT2C2-BFe2-BBC2	83(2)
BFe3-BFe1-BP	170.9(4)	AFe2-AFe1-AT1C2	83(2)	BT2C3-BFe2-BBC1	89(2)
		AFe2-AFe1-AT1C3	158(2)	BT2C3-BFe2-BBC2	93(2)
AFe1-AFe2-ABC1	86(1)	AFe2-AFe1-AT1C4	107(2)	BT3C1-BFe3-BT3C2	93(2)
AFe1-AFe2-ABC2	81(1)	AFe2-AFe3-AT3C1	129(2)	BT3C1-BFe3-BT3C3	97(2)
AFe1-AFe3-ABC1	83(1)	AFe2-AFe3-AT3C2	121(1)	BT3C1-BFe3-BBC1	175(2)
AFe1-AFe3-ABC2	84(1)	AFe2-AFe3-AT3C3	114(1)	BT3C1-BFe3-BBC2	89(2)
AFe2-AFe3-ABC1	46(1)	AFe3-AFe1-AT1C1	87(1)	BT3C2-BFe3-BT3C3	98(2)
AFe2-AFe3-ABC2	50(1)	AFe3-AFe1-AT1C2	86(2)	BT3C2-BFe3-BBC1	86(2)
AFe3-AFe2-ABC1	52(1)	AFe3-AFe1-AT1C3	101(2)	BT3C2-BFe3-BBC2	173(2)
AFe3-AFe2-ABC2	47(1)	AFe3-AFe1-AT1C4	164(2)	BT3C3-BFe3-BBC1	88(2)
BFe1-BFe2-BBC1	88(1)	AFe3-AFe2-AT2C1	131(1)	BT3C3-BFe3-BBC2	88(2)
BFe1-BFe2-BBC2	81(1)	AFe3-AFe2-AT2C2	118(1)	BBC1-BFe2-BBC2	91(2)
BFe1-BFe3-BBC1	85(1)	BFe1-BFe2-BT2C3	174(2)	BBC1-BFe3-BBC2	92(2)
BFe2-BFe3-BBC2	85(1)	BFe1-BFe3-BT3C3	170(2)		
BFe2-BFe3-BBC1	46(1)	BFe2-BFe1-BT1C3	148(2)	BFe1-BFe2-BT2C1	92(2)
BFe2-BFe3-BBC2	53(1)	BFe3-BFe1-BT1C3	92(2)	BFe1-BFe2-BT2C2	85(1)
BFe3-BFe2-BBC1	52(1)	BFe2-BFe1-BT1C1	88(1)	BFe1-BFe3-BT3C1	91(1)
BFe3-BFe2-BBC2	46(1)	BFe3-BFe1-BT1C1	84(1)	BFe3-BFe2-BT2C1	129(2)
		BFe3-BFe1-BT1C2	88(1)	BFe3-BFe2-BT2C2	120(2)
BFe2-BFe3-BT3C1	132(1)	BFe2-BFe3-BT3C3	108(2)	BFe3-BFe2-BT2C3	112(2)
BFe2-BFe3-BT3C2	121(1)	BFe2-BFe1-BT1C2	81(1)	BFe1-BFe3-BT3C2	88(1)

Figure 6. Bond angles in degrees

standard deviation of 0.05 Å calculated for the same type of distance from least squares. This indicates that our error estimates are fairly reliable and our errors are not underestimated. Since carbon is the lightest atom involved in any of the distances reported in this structure determination, any serious discrepancy would be expected to be evident here.

Discussion

The molecular structures of the two independent molecules are shown in Figure 7. Surprisingly, they are structural isomers of one another, an uncommon event but with some precedence (15). Also the presence of two isomers is consistent with the bridging C-O absorptions found in the infrared spectra (9) of $Fe_3(CO)_{11}P(C_6H_5)_3$. Two possible explanations which could be advanced to explain the occurrence of the two isomers in each asymmetric unit are that the two forms occur as dimers in solution or that packing is more favorable for the two isomers together than for either separately. The existence of dimers does not appear plausible since the shortest intermolecular distance in the crystal is 3.2 Å. At first glance, the packing argument also appears weak since it seems unlikely that the two isomers should be present in the proper proportions at the proper sites for crystallization to take place. However, the probability of this

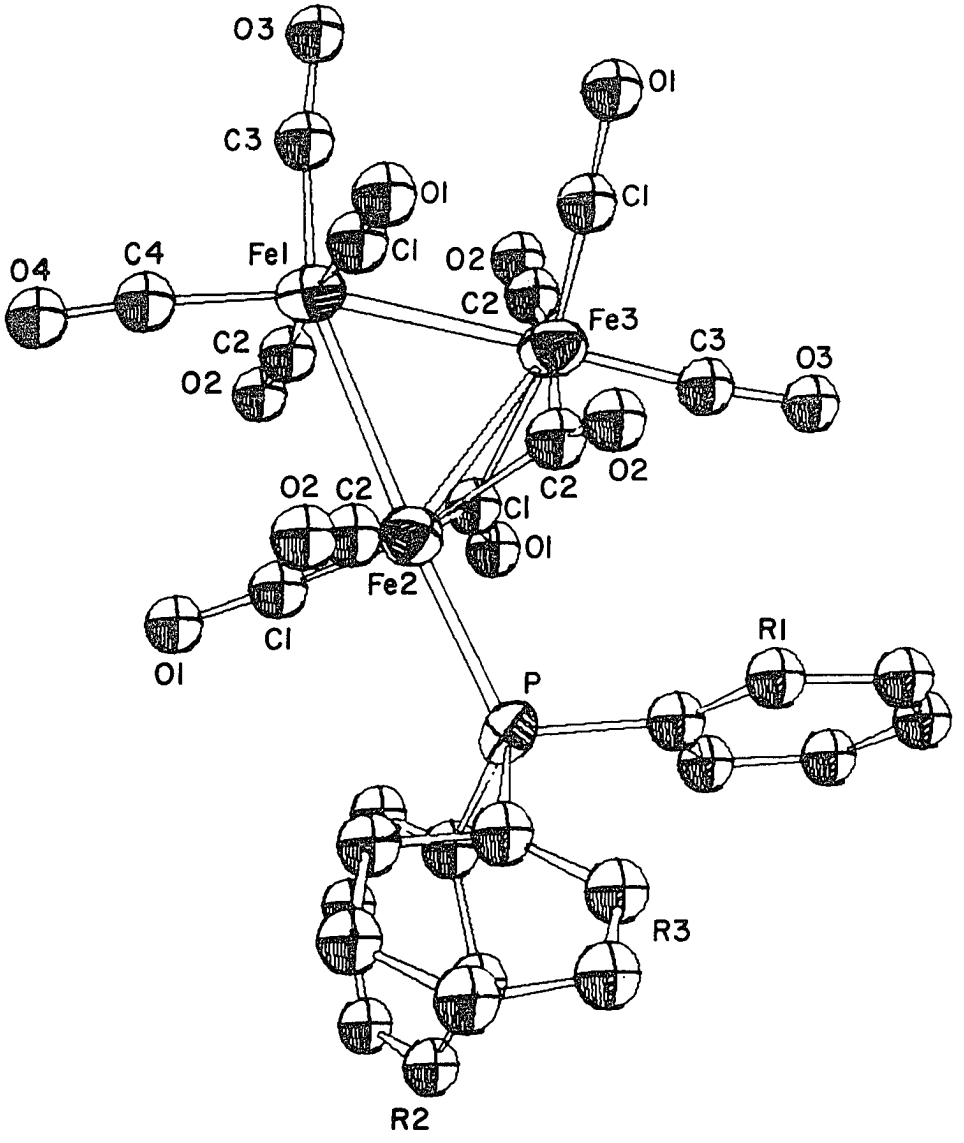

Figure 7. Molecular configurations of two isomers of $Fe_3(CO)_{11}P(C_6H_5)_3$

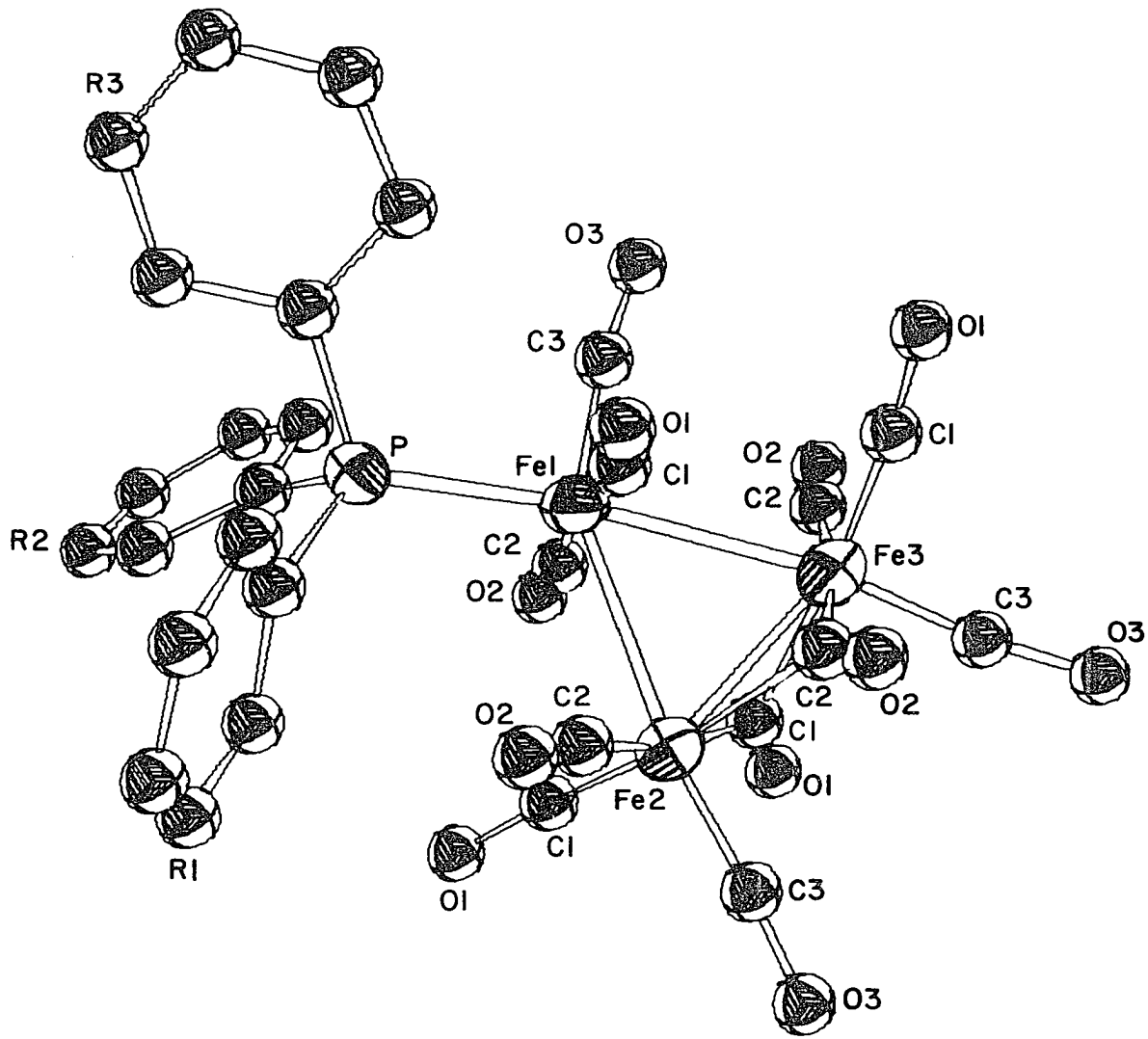

Figure 7. (Continued)

occurring would be increased if in solution the bridging bonds were continually being broken and the bridge was equally likely to reform between any two of the iron atoms. It is easy to see how the two molecules could be interconverted by this mechanism. This theory is made more palatable by the fact that the bridges are quite asymmetric and that the $P(C_6H_5)_3$ occurs in an equatorial position in both isomers.

The existence of asymmetric bridging in this structure is unquestionable. Three of the four bridges are asymmetric by more than three standard deviations and the fourth by more than two standard deviations. This asymmetry is consistent with the fact that the bridged iron-iron distances are greater than the 2.49 Å found (16) in $Fe_2(CO)_4(C_5H_5)_2$ or the 2.46 Å in $Fe_2(CO)_9$ in which the carbonyls form a nearly symmetric bridge (17). The iron-iron distances are similar to those found (8) in $HFe_3(CO)_{11}^-$ (2.577 Å for bridged; 2.685 and 2.696 for unbridged), but the reportedly symmetric bridge for that compound had only one bridging carbonyl and a bridging hydrogen.

Since both isomers of $Fe_3(CO)_{11}P(C_6H_5)_3$ show asymmetric bridging, it seems more likely that this is a property of the parent compound rather than an effect introduced by the $P(C_6H_5)_3$ group. On this basis the symmetry of an $Fe_3(CO)_{12}$ molecule would be C_2 instead of C_{2v} as previously proposed.

No asymmetry was found (11) in the bridging carbonyls in the redetermination of the structure of $Fe_3(CO)_{12}$, but any asymmetry in the bridges would be hopelessly hidden in the disorder which superposes terminal and bridging carbonyls. Asymmetric bridges might well occur in other previously determined structures but have not been recognized due to the presence of higher pseudosymmetry.

A comparison of the two isomers shows considerable variation in unbridged Fe-Fe bonds. The distance between two iron atoms, neither of which is bonded to a phosphorus atom, is similar to that found for unsubstituted $Fe_3(CO)_{12}$ (2.67 Å vs. 2.68 Å) while the Fe-Fe distances originating from the iron atoms which are bonded to a phosphorus atom are significantly longer. As described below, this lengthening might conceivably be due to increased population in antibonding orbitals. The bridged Fe-Fe bond is kept from lengthening extensively by the carbonyl bridges.

It might be expected that iron-carbon bonds opposite the longer bridging carbonyl bonds would be shorter than those opposite the shorter bridging bonds. Such variation would result from a weakening of the π-bond (and possibly also the σ-bond) in the lengthened bond and a consequent increase in the strength of the opposite bond, thereby causing a shortening. While it is impossible on the basis of statistics to say that the iron-carbon and carbon-oxygen distances in the terminal bonds are not all equivalent,

there does seem to be a more definite shortening in the iron-carbon bonds opposite the iron-iron bonds. Using the same arguments, the latter effect should occur and be larger than the former because there would be practically no π-character in the iron-iron bond. One would also expect lengthened carbon-oxygen distances in those cases where shortening of the iron-carbon distance has taken place. This effect in the present structure is somewhat masked by relatively large errors in lengths between the carbon and oxygen atoms, but the phenomenon is better illustrated by the nearly constant length for all iron-oxygen distances in spite of the more variant iron-carbon bond lengths.

The iron-carbon bond lengths around the iron atoms which are bonded to a phosphorus atom (av. 1.71) might in general be somewhat shorter than those around the other iron atoms (av. 1.73). If real, this could result from the inability of a $P(C_6H_5)_3$ group to compete with carbonyls as π-electron acceptors as effectively as the carbonyl which it replaces. Such shortening has previously been evidenced by a lower C-O stretching frequency for unsubstituted metal carbonyls than for the corresponding mono-substituted triphenylphosphine derivative (18). Angelici has proposed (19) that there is a transfer of electron density from the metal-phosphorus σ-bond to the metal-carbon π-bond.

Such transfer would also cause a decrease in metal-carbon bond length.

Several of the Fe-C-O angles vary considerably from 180°. This is frequently observed in lower symmetry systems (20) and can be attributed to steric and packing considerations.

The temperature factors of the carbonyl atoms are somewhat large as might be expected from the rapid fall off of intensity. It is not surprising that the oxygen atoms at the end of the carbonyls have larger temperature factors than the carbon atoms to which they are bonded. The ring carbon atoms have considerably smaller temperature factors and in every ring the carbon atom bonded to the phosphorus has a smaller temperature factor than the other atoms in the ring.

In a molecule of this complexity it is indeed hard to distinguish between causes, primary effects, and secondary effects, but the overall trends found in the structure do not seem unexpected in the light of present understanding.

In view of the widespread differences of opinion as to the interpretation of experimental results for the structure of $Fe_3(CO)_{12}$, it would be interesting to see if the most nearly correct structure could have been picked from those shown in Figure 1 from theoretical arguments. The treatment presented here by no means constitutes a rigorous

proof and, of course, was aided by the knowledge of the structure of $Fe_3(CO)_{12}$.

We will assume that in the correct structure the bonding will be such that all iron atoms will attain the krypton configuration, and that no iron atom will be bonded to more than seven other atoms. The first assumption is known to hold true for the vast majority of metal carbonyls, and the second seems reasonable for an atom the size of iron.

In the linear arrangement the center iron atom does not attain a filled shell with or without bonds being formed between iron atoms. If iron-iron bonds are formed, the center iron atom has eight bonds; if not, none of the iron atoms attain a filled shell. In fact, no linear arrangement which satisfies both assumptions is readily apparent.

A triangular arrangement with six bridging carbonyls seems less likely than a linear arrangement on the basis of valence bond and spatial arguments. Three iron-iron bonds are necessary for the iron atoms to fill their shells, but such bonding gives each iron atom eight bonds. In addition, this arrangement cannot be accomplished by use of the metal's $\underline{d^2sp^3}$ orbitals which are so frequently used in metal-carbonyl bonding.

On the basis of the above assumptions, triangular arrangements with either zero or two bridging carbonyls seem equally likely. A molecular orbital treatment was

carried out to see if one of these could be ruled out on the basis of energy requirements. The method used was very similar to one described for benzene (21). Each Fe-C bond was assumed to use a $\underline{d^2sp^3}$ orbital from an iron atom and only the remaining $\underline{d^2sp^3}$ and $\underline{d}$ orbitals from the iron atoms were used to form the molecular orbitals which can be thought of as holding the iron atoms together. The values of the resonance integral representing interactions between pairs of atomic orbitals were assigned symbols and ranked qualitatively on the basis of examination of a ball and stick model.

The molecule with no bridging carbonyls would have D_{3h} symmetry. Of the total 48 bonding electrons and 27 iron orbitals, the iron-carbon σ-bonds would use 24 electrons and 12 iron orbitals, leaving 24 electrons to be placed in 15 molecular orbitals. Our calculations showed that 7 of these orbitals would be bonding and 8 antibonding. This model seems unlikely in view of the number of electrons which must be placed in quite antibonding orbitals.

The molecule with two bridging carbonyls was treated as having C_{2v} symmetry. The iron-carbon bonds take up 28 electrons and use 5 orbitals each from two iron atoms and 4 from the other. This leaves 20 electrons to be placed in 13 molecular orbitals. In setting up the calculations, it was apparent that two types of interactions where atomic

orbitals from two iron atoms were nearly colinear would give a much larger value for the resonance integral than other interactions where atomic orbitals formed angles considerably less than 180°. Initially all of the small resonance integrals were assumed to be zero. This model gave 3 bonding orbitals, 3 very antibonding orbitals, and 7 nonbonding orbitals. Thus this model would appear to be energetically feasible, inasmuch as none of 20 electrons need be put in antibonding orbitals.

It should be noted that in the above calculations, it has been assumed that all Fe-C bonds are σ-bonds with a bond order of 1, and all π-bonding has been neglected. Also the interactions which were neglected could, no doubt, be used to break the degeneracy of the non-bonding orbitals. Such crude approximations might suffice for checking the feasibility of a certain structure, but we recognize their limited application for a detailed description of electronic arrangement.

A treatment of the correct structure which did not neglect most of the small interactions was also carried out. In this case the energy of the orbitals which had been bonding and antibonding before was unchanged, but the 7 nonbonding orbitals became 3 bonding and 4 weakly antibonding orbitals.

There are several p orbitals on carbon atoms which have the proper symmetry to π-bond with the iron atoms. Therefore it seems reasonable that much of the electron density in these iron-iron antibonding orbitals will be transferred to iron-carbon π-bonds, thereby increasing the net strength of the iron-iron bonds. If one then replaces a carbonyl with a lesser π-bonding triphenylphosphine, these antibonding orbitals should be given additional electron density. This would weaken the iron-iron bonds and result in the longer iron-iron distances noted in this structure determination.

THE DESIGN, INSTALLATION, AND AUTOMATION OF A NEUTRON DIFFRACTION SYSTEM

General Description of System

An automatic neutron diffraction system has been made operational at the Ames Laboratory Research Reactor. The system consists of several parts: a monochromating system, a diffractometer, an interface, a teletype, neutron counting devices, and a computer.

The monochromating system uses a beryllium crystal and yields a beam with virtually no higher order contamination. The diffractometer is a Hilger-Watts (model 4230-1) four circle device which operates under computer control (22). The computer used is an SDS-910 with 16K words of core storage. Auxiliary storage of five million words is provided by two magnetic disks. High speed access to auxiliary storage is provided by an IBM-1401 computer, which handles the flow of information between the main computer and the disks.

Programs for this computer system are written in the "TASK" language (23, 24) which is an "ALGOL" based language with several modifications to permit real time usage of the computer. The interaction between the computer and the diffractometer is through an interface, which carries out computer commands and relays information from the

experiment to the computer, as well as handling flow of information between the computer and the teletype. The teletype is the only means of communication a user has with the computer.

Design of Monochromating System

The neutrons in the core of the reactor are of a wide energy range but in general have higher than optimum energy for use in neutron diffraction. To increase the number of useful neutrons, the average energy of the neutron beam must be reduced before one energy is selected by the monochromating crystal. The design of the system used to moderate and monochromate the neutron beam which comes from the reactor core is illustrated in Figure 8.

The beam tube for the main beam is a circular opening 6 in. in diameter in the reactor wall running from the reactor core toward a cavity just inside the reactor face. Each end of the beam tube is covered with a 1/16 in. aluminum plate to make the tube air tight. Next to the interior aluminum plate is a 2 in. layer of graphite moderator through which all neutrons must travel. Through the remainder of the beam tube there is a 1 in. square opening through which neutrons traveling in a straight line from the reactor core to the monochromating crystal can pass freely. The small opening is surrounded for the first 22 in. by graphite, which "funnels" some additional neutrons

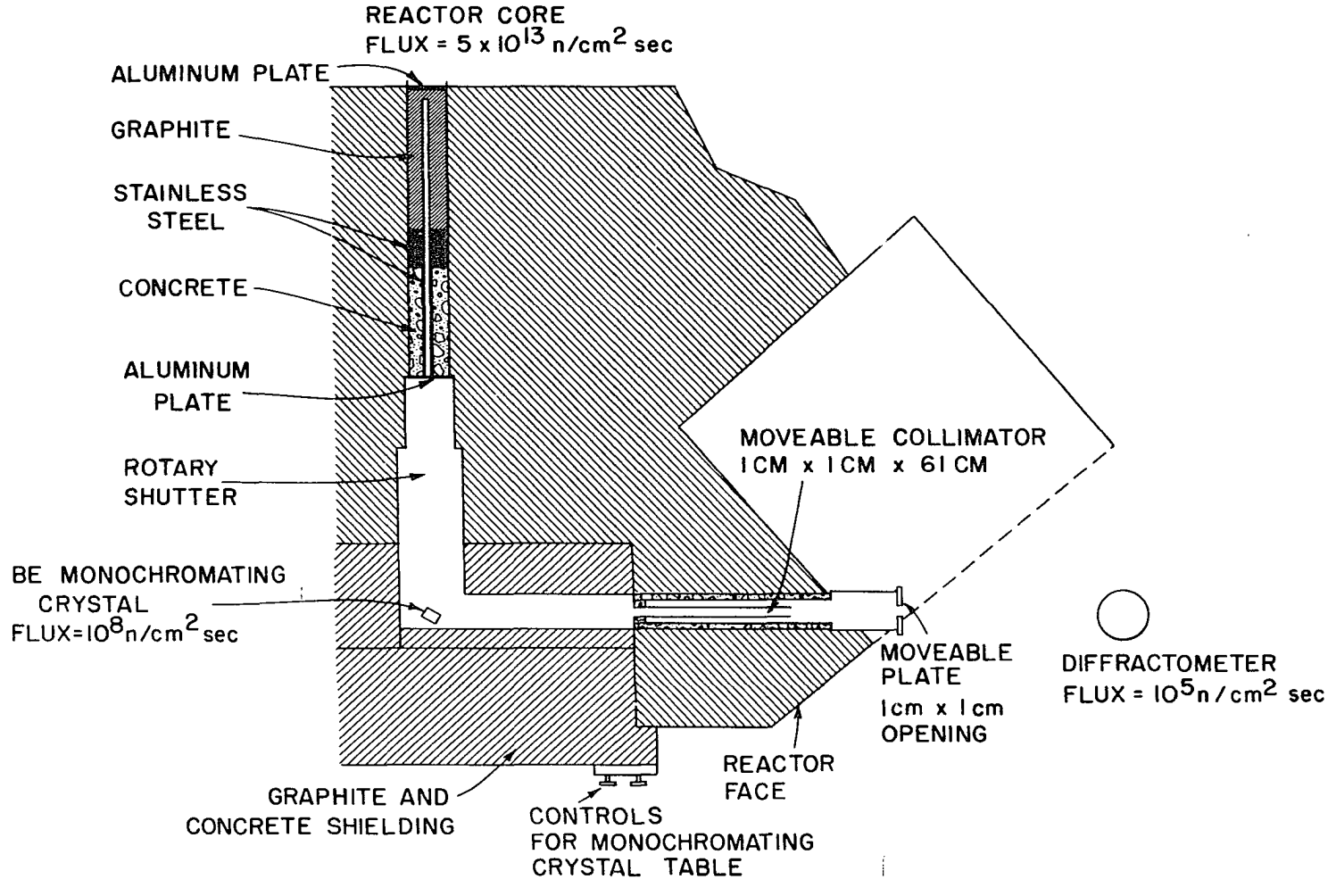

Figure 8. Moderating and monochromating system

into the opening. For the next 24 in. the opening is surrounded by stainless steel and concrete, which serve as a collimator for the main beam.

The position of the monochromating crystal is somewhat different than in many other systems. A common arrangement is to allow the main beam to impinge on a monochromating crystal external to the reactor face. This necessitates that considerable shielding be put up around the monochromating crystal and therefore takes up much floor space. It has an advantage in that it permits the angle between the beam incident to and diffracted from the monochromating crystal to be easily changed; consequently the wavelength being used can be optimized for a particular experiment. Our monochromating crystal, however, is located inside the reactor face, as illustrated in Figure 8. This arrangement requires that there be almost no shielding on the reactor floor but restricts the angle between the diffracted incident beam to approximately 90°. We will refer to this angle as the "take-off angle". Our take-off angle is large compared to that in many systems, but this is advantageous for data taking. All reflections from the sample crystal which occur at an angle less than the take-off angle have the same peak shape as the reflection from the monochromating crystal, but reflections which occur at angles higher than the take-off angle have a half-width greater than the half-width of the peak from

the monochromating crystal.

Our large take-off angle was an important factor in choosing beryllium for our monochromating crystal. Beryllium not only has a high scattering cross section, but also has a large Debye temperature and therefore the decrease of intensity due to thermal motion as a function of the take-off angle is smaller for beryllium than other metals. This is especially important at our large take-off angle.

All reflections of beryllium for which $h-k=3n$ and $\ell=2n$ have all beryllium atoms scattering in phase. Thus any one of these will have maximum intensity, so the only criterion for picking one is that Θ be 90° for a wavelength of approximately 1 Å. The $\bar{1}24$ reflection satisfies this condition and is the one currently being used.

The original specifications for the monochromating crystal called for a Be single crystal 1.5 x 1 x 0.5 in. cut with the 1.5 in. x 1 in. face parallel to the 001 plane. A 1 in. x 0.5 in. face was to be cut parallel to the 100 plane. The $\bar{1}24$ plane forms an angle of about 25° with the 001 plane, so that this Fankuchen cut would result in a decrease in the divergence of the beam. The crystal actually being used has a volume nearly twice that specified, but it is irregularly shaped so that its minimum dimensions are slightly smaller than specified. The face of the crystal being struck by the incident neutron beam is the 001 plane, and the 100 plane is placed horizontally.

The monochromating crystal is positioned on a mount inside the reactor face. This mount can be rotated 5°, tilted 10° and moved up to 1 in. in two horizontal directions by dials on the reactor face. The base beneath the mount can be similarly rotated by as much as 90°.

The collimator through which the neutrons pass from the monochromating crystal to the reactor face is housed in a concrete-lined steel tube about 6 in. in diameter. The collimator itself is a cadmium-plated steel tube 1 cm square and 61 cm long. The collimator can be driven by a motor from one side of the large tube to the other in a 3° arc which centers on the monochromating crystal. Because this system was designed exclusively for single crystal structural studies, fine collimation of the neutron beam is not necessary. However some additional collimation is provided by a moveable cadmium-filled brass plate with a 1 cm square opening. This plate slides over the end of the steel tube just at the reactor face.

The exact placement of the collimator is actually rather arbitrary, but the angle it makes with the incident beam does determine the exact wave length of the neutrons which enter the collimator. The line following the center of the collimator will be the "reference line" for the entire system. The monochromating crystal, the sample crystal, and the center of the instrument must lie on this line. The collimator was placed horizontally and was

centered on the approximate center of the monochromating crystal table. In order to facilitate later optical alignment of the orienter, two scribe marks identifying the reference line were made with the aid of a transit, one on a wall at the height of the collimator and a second on the floor near the reactor face directly below the reference line.

There is a small cadmium-plated shutter which, when activated by a selenoid, stops about 90 $^{o}/o$ of the monochromatic neutron beam. Complete cessation of the beam is accomplished by means of a large rotary shutter which can be closed to prevent the main beam from hitting the monochromating crystal. This large shutter, however, is not under computer control.

Alignment of Monochromating Crystal

In order to properly position the monochromating crystal, a BF_3 neutron detection system was placed on the reference line. The monochromating crystal was aligned by successively maximizing the intensity of the neutron beam with respect to the above mentioned adjustments of the monochromating crystal mount in a cyclic fashion until an absolute maximum was attained. Then the moveable plate was placed over the end of the steel tube. It was positioned optically and also so that the neutron intensity emerging from the opening was maximized.

After alignment is obtained, the rotation adjustment rotates the crystal about an axis perpendicular to the plane defined by the main beam and the diffracted beam. A curve obtained by measuring the intensity of the diffracted beam as a function of rotation indicates the mosaic spread of the monochromating crystal. The curve obtained for our beryllium crystal (Figure 9) shows the mosaic spread to be 0.41°.

Intensity of Diffracted Beam

While relative numbers of neutrons are easy to measure with uncalibrated BF_3 counters, exact intensities are not because BF_3 tubes are in general less than 100 °/o efficient. In order to determine the exact intensity of our beam and to get an idea of the efficiency of our BF_3 tube, a circular piece of gold foil 1 cm in diameter was placed in the diffracted beam. After irradiation for 19 1/2 hours with reactor power at 5 MW, the radioactivity of the gold was measured and the neutron flux was calculated. The result, 9.3×10^4 neutrons/cm^2 sec, was very close to that which we measured with our BF_3 counter, indicating that our BF_3 tube is nearly 100 °/o efficient.

Beam Uniformity and Divergence

The beam uniformity and divergence were recorded photographically. The intensifying screen was removed from a conventional Polaroid x-ray attachment and was

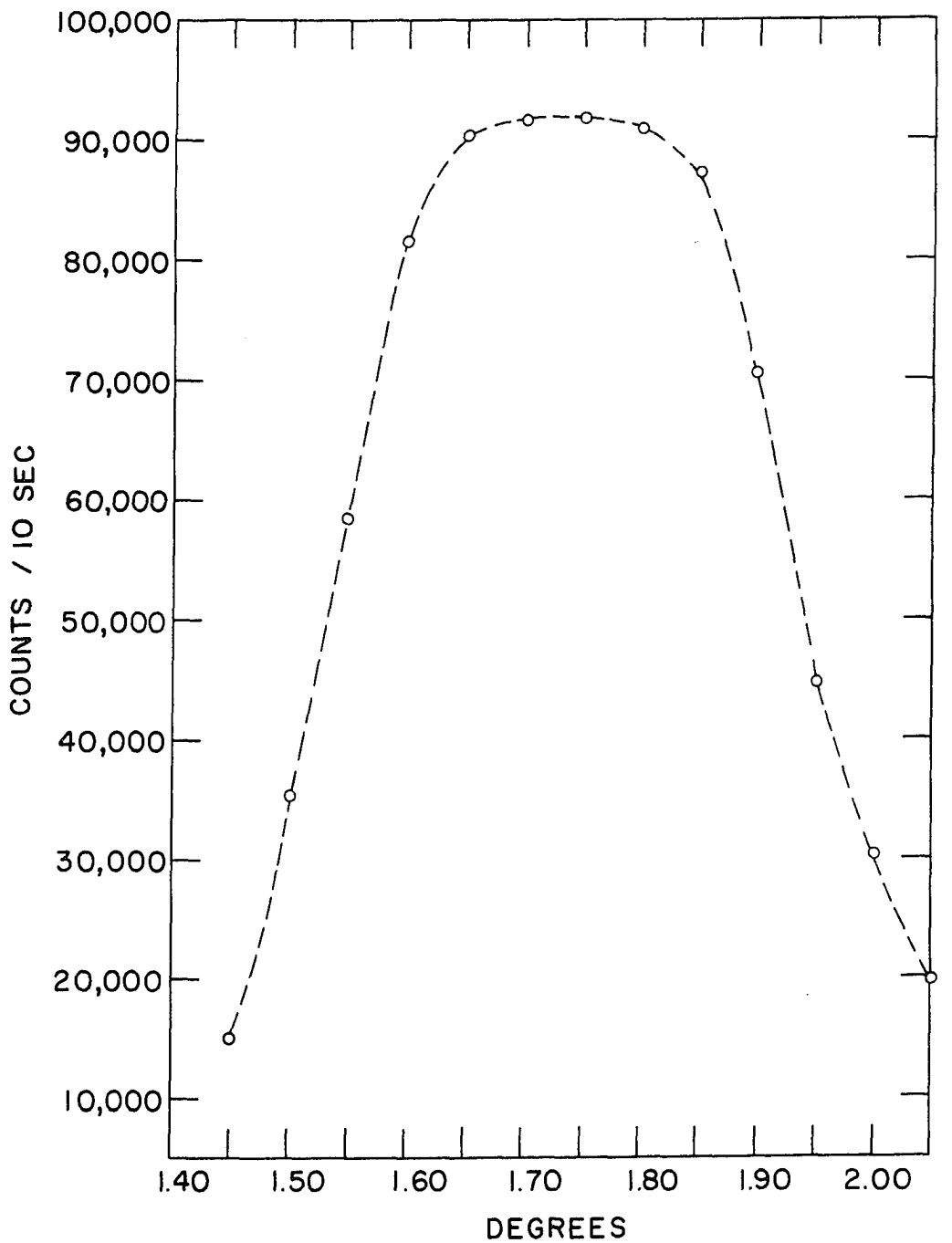

Figure 9. Rocking curve of beryllium crystal

replaced by a screen which emits light when struck by a neutron. The camera was placed next to the moveable plate, just outside the reactor face. As expected, the exposed portion of film was 1 cm square. An exposure was also made at a distance of 116 cm from the plate. Here the exposed portion measured 2.3 cm square indicating that the beam intensity falls off as the square of the distance plus 90 cm from the plate. In our present setup the crystal is 125 cm from the plate. From pictures made with several different exposure times, it was evident that the beam is quite uniform except at the extreme edges.

Determination of Higher Order Contamination

Ideally, the beam leaving the collimator should be one and only one wave length. This is usually impossible to obtain because of second or higher order contamination. If a set of h, k, ℓ planes of monochromating crystal are in position to diffract neutrons of wave length λ into the collimator, the nh, nk, nℓ planes will be in position to diffract neutrons of wave length λ/n in the same direction, and higher order contamination will result. One could reduce the problem by choosing a reflection which has an extinct second order reflection, but this is impossible for beryllium if one desires a first order reflection of highest intensity.

The amount of higher order contamination was determined by a time of flight analysis of the diffracted beam. A chopper which lets neutrons pass intermittently was placed in the beam at the collimator with a BF_3 detector positioned 43.53 meters from the chopper. The length of time which the chopper was open was short enough to give adequate resolution, and the time it was closed is long compared to the time it takes a 1 Å neutron to travel from chopper to detector. When the chopper was open a pulse was generated and t seconds later the counting system was turned on for 0.04 milliseconds. For each value of t, this process was repeated for 100 seconds. A plot of the number of counts as a function of flight time is shown in Figure 10. From this it can be seen that the amount of higher order contamination is less than 1 %.

Design of Orientation System

The table on which the diffractometer sets has translations in two perpendicular horizontal directions and a height adjustment. The table was bolted to the reactor floor so that its center was very close to the reference line and so that one of the translational adjustments on the table was perpendicular to the reference line.

The instrument itself is a device for positioning a crystal in any orientation. A crystal can be mounted on a standard goniometer head which can be affixed onto the

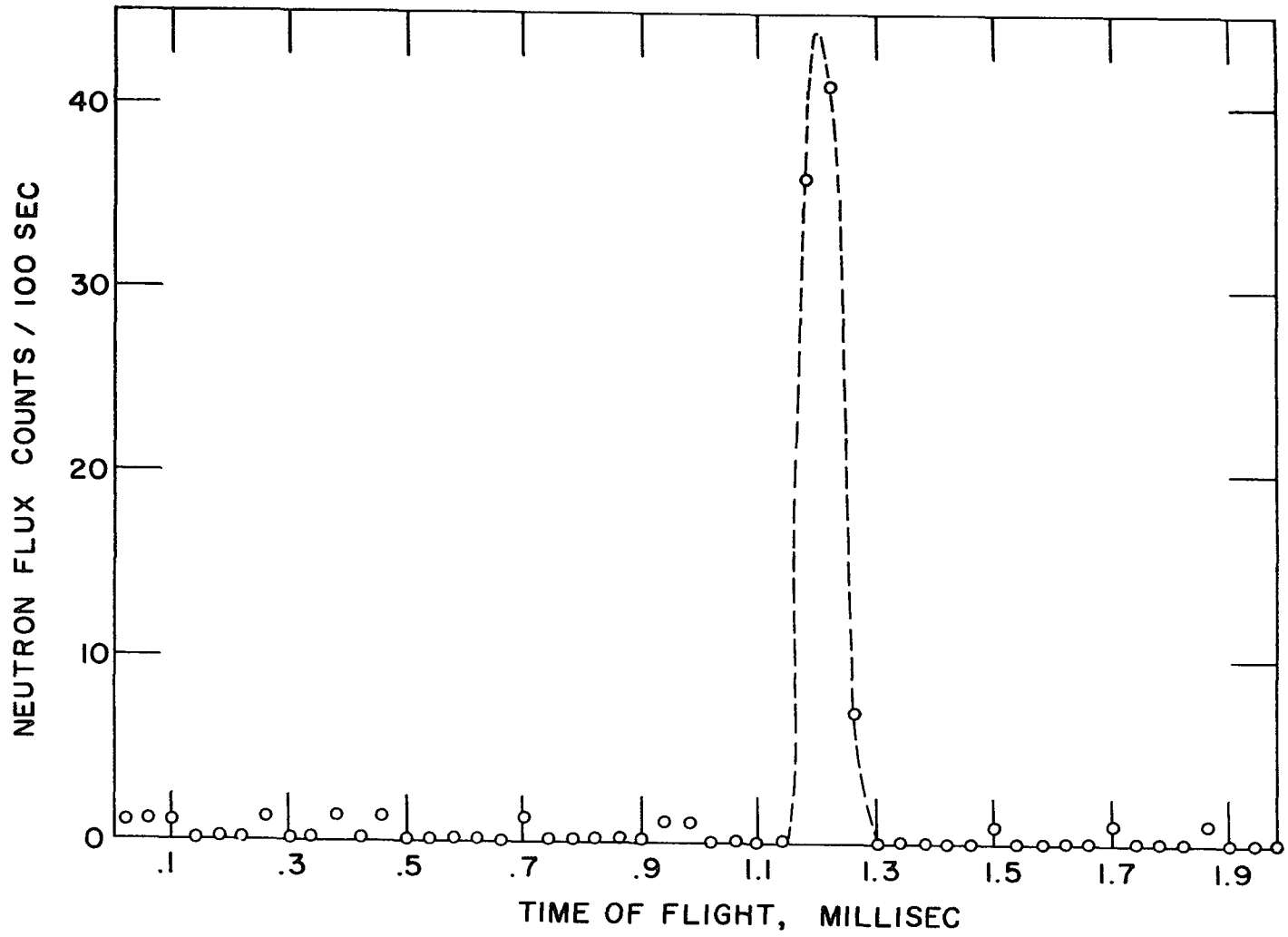

Figure 10. Wavelength analysis of beam

instrument by means of a screw fitting. The crystal can then be rotated about any of three axes, designated as phi, chi, and omega. The detector arm rotates about an axis designated as the theta axis.

When all axes are at their zero positions, the theta, omega, and phi axes are vertical, and the chi axis is horizontal and parallel with the reference line. The direction of positive rotation is counterclockwise, looking down in the case of theta, omega, and phi, and toward the monochromating crystal for chi, when all other axes are at their zero positions.

In the following discussion, the term "axis" will be reserved for the axis about which the crystal is rotated. The term "shaft" will refer to the mechanical assembly which moves when rotation about an axis occurs. The symbols χ, ω, and Φ will be reserved to indicate the number of degrees the corresponding shaft has been rotated from its zero position. The symbol Θ will represent one-half the number of degrees the detector arm has been rotated from its zero position. The term "value" of a shaft will have the same meaning as the Greek symbols.

The shafts are positioned by a moiré fringe method. To accomplish this, each shaft has a radial transmission grating which generates fringes as it passes over a fixed grating on a pick-up head which also contains a lamp and photocells. Movements of the fringes produce pulses which

can be counted by the computer so that in the ideal case shaft position is known to 0.01°. This method of pulse counting necessitates an absolute datum point or external reference for shaft position. In order to prevent the accumulation of errors, the shafts must periodically be returned to their datum points. The location of a datum point to within 0.01° is facilitated by a reference mark on each shaft's grating which is detected by a separate pick-up head. In order to find its datum point, a shaft can be operated in a "datum seek" mode. When the datum point of a shaft moving in datum seek mode passes the second pick-up head, the shaft stops moving and a pulse (interrupt) is produced. Exact positioning of shafts when the instrument is operated manually has been found to be extremely difficult. The instrument can be effectively operated manually in the datum seek mode, however.

Each shaft except phi has limit switches to protect the instrument from damage. Over 360° rotation is provided for omega, just under 360° for chi, and about 210° rotation for the detector.

The detector shielding provided by the instrument's manufacturer was found to be inadequate. Therefore a new receiving collimator and the surrounding detector shield is currently being constructed.

Detector System

If relative intensities of reflections from a sample crystal are to be measured, it is important that there be the same number of neutrons in the beam incident to the crystal while both reflections are being measured. Since the neutron flux from the reactor is not steady over long periods of time, it is not sufficient to make each measurement for the same length of time. For this reason, the beam passes through a fission chamber just before it gets to the sample crystal. This chamber contains a thin layer of U^{235}. About 1 neutron in 1000 causes a U^{235} atom to split, and this generates an electronic pulse. This pulse is amplified by a preamplifier and sent into the interface for recording as described later. The number of these pulses is directly proportional to the beam flux so that instead of measurements being made for a fixed length of time as in x-ray diffraction, they are made for a fixed number of monitor counts.

The intensities are recorded by means of a BF_3 tube inserted into the receiving collimator. When a neutron is captured in the tube a pulse is generated which is amplified by a preamplifier, sent through an amplifier-discriminator and then into the interface.

Under current operating conditions a voltage of 2650 volts is placed on the BF_3 tube, and 500 volts on the fission chamber. The gain of the preamps is about 3×10^{12} volts/coulomb with a noise level of less than 0.25 volts.

The pulse leaving the integrating preamplifier caused by a typical neutron in the fission chamber is 1 volt. In the BF_3 tube, the corresponding pulse is also 1 volt, while a gamma ray gives a pulse of less than 0.3 volts. The amplifier-discriminator sends out a 10 volt pulse for every pulse over 0.4 volts which it receives.

Optical Alignment of Instrument

In order to facilitate optical alignment of the diffractometer, a round lead shot was mounted on a goniometer. The ball was placed on the phi axis of rotation by adjusting the translations on the goniometer. It was placed on the chi axis of rotation by using the height adjustment of the orienter. The shot was assumed to be on an axis if displacement of the center of the shot as the axis was rotated was not detectable through a transit. If the diffractometer has been constructed correctly, after the above operations the center of the shot would also be on the omega axis. However, when the omega axis was rotated 180°, the center of the lead shot moved noticeably. The phi axis was moved by loosening the four screws which hold the phi carriage to the chi carriage and, while pushing it in the proper direction, retightening them. After several attempts at this, the ball was put in a place where, to the accuracy of our observation, the position of its center was independent of the phi, chi or omega rotations. The center of the ball

was then at what shall be termed the "instrument center".

By making use of the transit and the aforementioned scribe marks, the translational and height adjustments of the instrument table were set so that the instrument center lay on the reference line. By sighting along the reference line, the receiving collimator was placed so that its center line fell on the reference line. This was accomplished by moving the theta shaft and adjusting setscrews provided on the detector base. Optical alignment of the instrument was then complete.

Alignment of Instrument Using Neutrons

Final alignment of the instrument was accomplished after automation was complete by finding the exact peak positions of a few reflections from a zinc crystal. The crystal was mounted so that a prominent reflection was in position to diffract when chi was at 90°. If the reciprocal axis of a crystal is parallel with the phi axis of our instrument, the reflection on this axis is independent of a phi rotation when chi is at 90°.

The settings of the four shafts which maximized the intensity of the reflection in the detector were found by a "half peak" method. In this method, the four shafts are set so that their placement is approximately correct to have the reflections strike the detector. In a cyclic, iterative process the settings of the omega, theta, and chi shafts are

found which maximize the peak in the detector relative to the positions of the other shafts.

The process of maximizing with respect to one shaft is started by taking a count somewhere near the peak maximum. The two settings (one on each side of the peak) of the shaft which give 1/2 of this count are located to the nearest 0.01°. The shaft is set at the average of these two settings and the next shaft is maximized in the same manner. In practice, two cycles of the three shafts give convergence.

If both the instrument and crystal are centered and if the interplanar spacings are such that the Bragg angle is θ, the reflection should be centered at the instrument settings shown in Table 3.

The exact shaft positions which center the peak near these settings are determined. The deviations of the exact settings from those in the table are due to errors in arc and translational adjustments on the goniometer, crystal height, or misalignment of the instrument.

In order to minimize the effect of errors in crystal alignment, the settings are averaged in the following manner. The a and b positions of each setting are averaged to give a new theta, omega, and chi which are independent of goniometer setting errors.

Next the theta and chi positions of pairs 1 and 5, 2 and 6, 3 and 7, and 4 and 8 are averaged. The omega positions of these are also averaged after subtracting 180° from the

Table 3. Equivalent instrument settings

Position	Theta	Omega	Chi	Phi[a]
1a	θ	θ	90	p
1b	θ	θ	90	180+p
2a	θ	θ	-90	p
2b	θ	θ	-90	180+p
3a	-θ	-θ	90	p
3b	-θ	-θ	90	180+p
4a	-θ	-θ	-90	p
4b	-θ	-θ	-90	180+p
5a	θ	180+θ	90	p
5b	θ	180+θ	90	180+p
6a	θ	180+θ	-90	p
6b	θ	180+θ	-90	180+p
7a	-θ	180-θ	90	p
7b	-θ	180-θ	90	180+p
8a	-θ	180-θ	-90	p
8b	-θ	180-θ	-90	180+p

[a]The value of phi is arbitrary.

omega settings in 5, 6, 7, and 8. The resultant values are independent of errors in crystal height and will be termed the +++, ++-, --+, and --- solutions, respectively.

The chi values from the +++ and --+ solutions are averaged as are those from the ++- and --- . We will term these values $\chi+$ and $\chi-$, respectively. The average of $\chi+$ and $\chi-$ is the instrument setting of the chi shaft which corresponds to the true zero position of the shaft. The chi values for all four solutions can then be corrected for errors in the zero position. If the average height of the neutron sensitive portion of the detector is correct, all values of chi should have a magnitude of 90°. If the detector is too low, the magnitudes of chi for the +++ and --- solutions are greater than 90° and for the --+ and ++- solutions are less than 90°. If the detector is too high, the opposite effect is observed.

The theta and omega values of the +++ and --+ solutions can be averaged to give the instrument settings which correspond to the true zero positions of the theta and omega shafts. The same can be done for the ++- and --- solutions. If the omega zero position obtained from this averaging is different from that obtained from the first, it would indicate that the four instrument axes do not have a common point.

In practice, after these determinations are completed, the corrections indicated are made and the process is performed again. From what has been said, it might not seem necessary to correct the crystal position but this is done as a precaution (lest crystal position errors might not be cancelled by the averaging process as they should be in theory) and because it is a great aid in determining whether a line passing lengthwise through the center of the detector intersects the four axes at the instrument center. When a crystal is at the instrument center and all shaft settings are such that the peak maximum is falling on the detector, it should be falling on the center of the detector. This is easily confirmed by using the up-down and left-right beam splitters, which can be operated either manually or under computer control. When the detector is properly positioned, alignment of the instrument is complete.

The Interface

The interface has several 24 bit registers. These registers can be loaded or read by a program being executed in the computer. The TASK language statement which causes a register to be read is of the form:

.INPUT. (A,B);

where both A and B can be either a number or a program variable. After execution of this statement, register A will contain the value of B.

The registers in the interface of the experiment being described have been assigned numbers 64-73. There are more numbers than there are registers because two different numbers can refer to the same register.

The number whose binary representation is contained in a 24 bit word or register is the value of that word. Three of the interface registers are used for counting pulses and therefore have a value with intrinsic meaning. The values which represent the contents of the other registers are arbitrary and have only the meaning given them by the design of the interface. For example, if a bit of a certain register is set equal to 1, the theta shaft will begin moving, or when a shaft hits a limit switch, a bit reserved for that shaft is set equal to 1. The meaning of all bits which a programmer or experimenter might need to know are summarized in Table 4. Table 5 shows the action taken on all .INPUT. and .OUTPUT. statements which the computer could address to the interface of the experiment being discussed.

Another means of sending information to the computer is by 11 interrupt lines. Eight of them are special interrupt lines. These are used in keeping track of the position of the four axes. Each shaft has two special interrupt lines running to the computer. Every time a shaft moves 0.01° in the positive direction a pulse is sent on one of the two lines, the computer halts what it is doing, adds 1 to the value stored in the location reserved for the position

Table 4. Register meanings

Register	Bits	Meaning
1	0	Phi is at datum
	1	has no meaning
	2	Phi is in datum seek mode
	3	Phi is in positive drive
	4	Phi is in fast drive
	5	Phi is moving
	6	Chi is at datum
	7	has no meaning
	8	Chi is in datum seek mode
	9	Chi is in positive drive
	10	Chi is in fast drive
	11	Chi is moving
	12	Omega is at datum
	13	Omega is in step-scan mode
	14	Omega is in datum seek mode
	15	Omega is in positive drive
	16	Omega is in fast drive
	17	Omega is moving
	18	Theta is at datum
	19	Theta is in step-scan mode
	20	Theta is in datum seek mode
	21	Theta is in positive drive
	22	has no meaning
	23	Theta is moving
2	0-23	Binary representation of time pulse counter
3	0-23	Binary representation of detector counter

Table 4. (Continued)

Register	Bits	Meaning
4	0-23	Binary representation of monitor counter
5	0	Request for counting to begin
	1	Permits counters to restart during step-scan
	2	Counting will stop when monitor counter reaches zero
	3	Counting will stop when detector counter reaches zero
	4	Counting will stop when time pulse counter reaches zero
	5	Counters are operating
6	12	Set time pulse counter to zero
	13	Set detector counter to zero
	14	Set monitor counter to zero
	18	Set all counters to zero, stop all shafts, and disengage all beam splitters
	19	Reset limit switch indicators
7	12	has no meaning
	13	has no meaning
	14	Phi has hit its limit switch
	15	Chi has hit its limit switch
	16	Omega has hit its limit switch
	17	Theta has hit its limit switch
	18	has no meaning
	19	Right beam splitter is engaged
	20	Left beam splitter is engaged
	21	Bottom beam splitter is engaged
	22	Top beam splitter is engaged
	23	Shutter is open

Table 5. Meaningful input and output statements

Statment	Bits	Experiment Register	Operation
.INPUT.(64,T);	0-24	1	The bits listed
.INPUT.(68,T);	0-24	2	of program variable
.INPUT.(69,T);	0-24	3	T will be given the
.INPUT.(70,T);	0-24	4	configuration of
.INPUT.(71,T);	0-5	5	the corresponding
.INPUT.(73,T);	18-23	7	bits in the Experiment Register listed.
.INPUT.(65,T);			Operation is not
.INPUT.(66,T);			defined; no action
.INPUT.(67,T);			is taken.
.INPUT.(72,T);			
.OUTPUT.(64,T);	19-23	1	The indicated
.OUTPUT.(65,T);	13-17	1	bits of the
.OUTPUT.(66,T);	8-11	1	Experiment Register
.OUTPUT.(67,T);	2-5	1	shown will be given
.OUTPUT.(68,T);	0-24	2	the configuration
.OUTPUT.(69,T);	0-24	3	of the corresponding
.OUTPUT.(70,T);	0-24	4	bits in the value
.OUTPUT.(71,T);	0-4	5	of T.
.OUTPUT.(72,T);	12-14,18-19	6	
.OUTPUT.(73,T);	12-23	7	

of the shaft, and then the computer goes back to what it was doing. If a shaft moves 0.01° in the negative direction, a pulse is sent on the opposite line of the pair and 1 is subtracted from the value in the shaft location address. These are called special interrupts because the computer always responds to them in the same way as determined by hardware circuitry. These interrupts are handled the same way regardless of what program is operating the experiment or, in fact, whether or not any program is being executed at all. A program can use any of these reserved locations as one of its variables and thereby know or even change the value of these locations but cannot respond directly to the interrupts.

The non-special interrupts, on the other hand, depend entirely on user programs for action to be taken when they occur. In the TASK language a program can ask to be informed of a particular interrupt and then take the necessary action. If an interrupt occurs of which no program has asked to be informed, it is ignored. These non-special interrupts occur to indicate that a shaft is at its datum position, to indicate that a shaft has hit its limit switch, or that some phase of neutron counting has ended.

To better illustrate the interaction of computer and experiment, two examples of typical processes are presented. In these examples, the underlined arguments of the .INPUT. and .OUTPUT. statments are given as binary numbers. In

reality, if numbers such as these are put into TASK language programs they would be given octal or decimal representations in the source language coding but upon execution would have binary representations in core.

Let us assume that ω is 50° and that a datum check of the omega shaft is desired. The first statement executed could be:

.OUTPUT. (65,11000000);

As can be seen by looking at Table 4, this would load bits 13-17 of register 1 with the values 0, 0, 0, 1, and 1, respectively. As shown by Table 2, the omega shaft would then begin moving fast in the negative direction. The program could then check periodically to see if ω was getting close to zero. When ω was found to be less than 5°, the program could execute the statement:

.OUTPUT. (65,1001000000);

and ask to be informed when the shaft reached its datum point. The execution of this statement would cause omega to move at slow speed in the negative direction in the datum seek mode. When omega reached its datum point, it would stop and an interrupt would be sent to the computer. Since the program has asked to be informed when this interrupt occurs, the program could go on to a subsequent task knowing that omega is at its datum point.

As a second example, assume a detector count is desired for 1000 monitor counts. The following statements could be

executed:

.OUTPUT. (72,100000);

.OUTPUT. (70,-1000);

.OUTPUT. (71,111000000000000000000000);

and the program could ask to be informed when the counting was complete. The first of these statements would cause the value of all three counters to be set to zero. The second statement would load the binary representation of a -1000 in register 4. The third statement would cause counting to begin when all three counters were ready, and counting would stop when 1000 counts had been accumulated in the monitor counter and its value became zero. When counting stops, an interrupt is sent to the computer and the program is informed that counting has been completed. The program could then execute the statement:

.INPUT. (69,A);

and the value of the program variable A would then be the number of detector counts accumulated while the counters were operating.

Structure of $NH_4V(SO_4)_2 \cdot 12H_2O$

Although each component of this neutron diffraction system was tested to some extent as it was installed, it was felt that an overall evaluation of the instrument could best be performed by trying it on a type of problem which exemplifies those for which the instrument would most

frequently be used.

The compound $NH_4V(SO_4)_2 \cdot 12H_2O$ was selected for a trial structural determination because it has several advantages. It is a member of a large group of compounds called alums, all of which readily form large crystals. The structures of several of these, isomorphous to $NH_4V(SO_4)_2 \cdot 12H_2O$, have been determined by x-ray diffraction (25), and the structure of $KCr(SO_4)_2 \cdot 12H_2O$ has been determined by neutron diffraction (26). Thus data collected could be immediately compared to that predicted by an approximate model, so that it would be readily apparent if the data were of poor quality. This could be done equally well by using a compound whose structure had been previously determined, but the obvious advantage of using a compound whose exact structure is unknown is that information of scientific value may result as a by-product of the test.

The structure of $NH_4V(SO_4)_2 \cdot 12H_2O$ was felt to be of interest in view of the dearth of structure determinations of V^{+3} compounds. It might be expected that the presence of a V^{+3} in the nearly octahedral environment which it has in this structure would cause distortion from that found in the corresponding Cr^{+3} structure. In an octahedral environment, there are two d orbitals with higher energy than the other three. In Cr^{+3}, all three of the low energy orbitals contain one electron. In V^{+3}, only two of the low energy orbitals

have an electron. Therefore a Jahn-Teller distortion would be expected, which would lower the energy of the populated orbitals and increase the energy of the unpopulated one. However, because these low energy orbitals are not pointing directly at any ligands, the distortion would be expected to be small.

Collection of Data

The diffraction data of $NH_4V(SO_4)_2 \cdot 12H_2O$ were collected under computer control. The shafts were set to record the intensity at the peak maximum for 5120 monitor counts. If the reflection was judged to be significantly above background, the theta and omega settings were offset by 0.50°, and a background was recorded for 2560 monitor counts. A 1.01° theta-omega coupled step scan was then initiated. At each step the intensity was recorded for 1024 monitor counts. The total integrated intensity was recorded, and another background measurement was made.

The backgrounds were found to be independent of angle settings beyond 5° in θ. Backgrounds for reflections within 5° were estimated from their individual background measurement. For reflections beyond 5°, the backgrounds were determined by averaging all the backgrounds which were at the same level.

There were two distinct background levels, depending on whether the neutron port adjacent to the diffractometer was

open. The port was being used by another experimental group to determine the energy distribution in an undiffracted neutron beam. Because their experiment was temporary, almost no shielding was installed, so the radiation level in the room was raised considerably.

The data were corrected for background, absorption, and the Lorenz factor. Standard deviations were calculated for each intensity by use of the expressions:

$$I = \text{COUNT} - \text{BACKGROUND}$$

$$\sigma I = \text{COUNT}\ (1 + \alpha) + (\sigma_{BG})^2$$

$$\sigma F = \frac{1}{L}\left[(I + \sigma I)^{1/2} - I^{1/2}\right]$$

where COUNT is the total integrated intensity of the peak, L is the Lorenz factor, σ_{BG} is the error in the BACKGROUND in this case calculated from the distribution of background counts at the same background level, and α is a constant included to take into account systematic errors in recording intensities.

Using the atomic positions found in the structure of $NH_4Al(SO_4)_2 \cdot 12H_2O$, refinement of the data converged at wR = 0.23. Isotropic temperature factors were then allowed to vary and while some of them were not well behaved, refinement to wR = 0.20 was attained. Attempts made at further refinement did not succeed. The atomic parameters which gave R = 0.26 were used to determine the signs of the observed structure factors and these were used as Fourier coefficients to calculate a map analogous to an electron

density map in x-ray diffraction. The z = 0 section of the map is shown in Figure 11. In Figure 12, the same map is shown including only peaks whose magnitudes are greater than the estimated noise level. This section of the map shows the coordination about a vanadium atom. The positions of the oxygen peaks would indicate that there is distortion from octahedral symmetry, but it is impossible to say that this is real with the agreement factor being at this level.

It was realized that poor agreement could be caused by an error in programming, indexing, or something similar, so such errors were looked for but none could be found. The alternative left is that the diffraction data are not of best quality. This does not seem unreasonable in view of the extremely high background counts encountered in data collection. Only about 10 $^{o}/_{o}$ of the reflections had a net count which was as large as the background.

This fact led to redesigning of the shielding around the neutron beam incident onto the sample crystal and around the detector. These modifications lowered the background by approximately a factor of 10 and should considerably improve the quality of the next set of data collected. This test determination indicated that the system was adequate in most other respects.

-312-259-194 72 9861237 331 -88 244 116-191-124-248-153 9741799 974-153-248-124-191 116 244 -88 3311237 986 72-194-259-312
-259 -72 -98 -9 585 685 -11-166 272 191-101 -19 -88-158 467 974 377-339-165 156 102 131 19-421-278 432 546 154 -17-139-259
-194 34 90 57 14-311-672-456 34 129 50 135 72-202-269-153-221-306 -87 158 123 6-121-377-476-199 80 53-156-300-194
72 19 -95 23 6-253-359-244-166-188-212-139 -5 -22-211-248 -60 16 -84-102 -51 -93-106 -39 -45 -18 94 -36-309-206 72
986 493 -98 -93 51 74 108 17-155-199-225-239 -65 90 -12-124 -7 88 -22 -56 87 90 -27 -2 36 -7 -31-128 -42 576 986
1237 835 207 -70-128 -65 -8-109 -97 104 118 -43 -91 -60 -96-191-211 -77 20 12 61 55 -86 -97 -15-100-246-254 82 8091237
331 325 202 16 -97 2 6-219-195 65 57-133-182 -80 85 116 -19 -27 8-146-268-286-320-147 148 122-100-154 -38 165 331
-88 -48 49 39 15 150 97-262-343-121-124-226-109 95 243 244 114 61 18-118-156-207-389-288 52 91 -44 -3 49 -23 -88
244 114 61 18-118-156-207-389-288 52 91 -44 -3 49 -23 -88 -48 49 39 15 150 97-262-343-121-124-226-109 95 243 244
116 -19 -27 8-146-268-286-320-147 148 122-100-154 -38 165 331 325 202 16 -97 2 6-219-195 65 57-133-182 -80 85 116
-191-211 -77 20 12 61 55 -86 -97 -15-100-246-254 82 8091237 835 207 -70-128 -65 -8-109 -97 104 118 -43 -91 -60 -96-191
-124 -7 88 -22 -56 87 90 -27 -2 36 -7 -31-128 -42 576 986 493 -98 -93 51 74 108 17-155-199-225-239 -65 90 -12-124
-248 -60 16 -84-102 -51 -93-106 -39 -45 -18 94 -36-309-206 72 19 -95 23 6-253-359-244-166-188-212-139 -5 -22-211-248
-153-221-306 -87 158 123 6-121-377-476-199 80 53-156-300-194 34 90 57 14-311-672-456 34 129 50 135 72-202-269-153
974 377-339-165 156 102 131 19-421-278 432 546 154 -17-139-259 -72 -98 -9 585 685 -11-166 272 191-101 -19 -88-158 467 974
1799 974-153-248-124-191 116 244 -88 3311237 986 72-194-259-312-259-194 72 9861237 331 -88 244 116-191-124-248-153 9741799
974 467-158 -88 -19-101 191 272-166 -11 685 585 -9 -98 -72-259-139 -17 154 546 432-278-421 19 131 102 156-165-339 377 974
-153-269-202 72 135 50 129 34-456-672-311 14 57 90 34-194-300-156 53 80-199-476-377-121 6 123 158 -87-306-221-153
-248-211 -22 -5-139-212-188-166-244-359-253 6 23 -95 19 72-206-309 -36 94 -18 -45 -39-106 -93 -51-102 -84 16 -60-248
-124 -12 90 -65-239-225-199-155 17 108 74 51 -93 -98 493 986 576 -42-128 -31 -7 36 -2 -27 90 87 -56 -22 88 -7-124
-191 -96 -60 -91 -43 118 104 -97-109 -8 -65-128 -70 207 8351237 809 82-254-246-100 -15 -97 -86 55 61 12 20 -77-211-191
116 85 -80-182-133 57 65-195-219 6 2 -97 16 202 325 331 165 -38-154-100 122 148-147-320-286-268-146 8 -27 -19 116
244 243 95-109-226-124-121-343-262 97 150 15 39 49 -48 -88 -23 49 -3 -44 91 52-288-389-207-156-118 18 61 114 244
-88 -23 49 -3 -44 91 52-288-389-207-156-119 18 61 114 244 243 95-109-226-124-121-343-262 97 150 15 39 49 -48 -88
331 165 -38-154-100 122 148-147-320-286-268-146 8 -27 -19 116 85 -80-182-133 57 65-195-219 6 2 -97 16 202 325 331
1237 809 82-254-246-100 -15 -97 -86 55 61 12 20 -77-211-191 -96 -60 -91 -43 118 104 -97-109 -8 -65-128 -70 207 8351237
986 576 -42-128 -31 -7 36 -2 -27 90 87 -56 -22 88 -7-124 -12 90 -65-239-225-199-155 17 108 74 51 -93 -98 493 986
72-206-309 -36 94 -18 -45 -39-106 -93 -51-102 -84 16 -60-248-211 -22 -5-139-212-188-166-244-359-253 6 23 -95 19 72
-194-300-156 53 80-199-476-377-121 6 123 158 -87-306-221-153-269-202 72 135 50 129 34-456-672-311 14 57 90 34-194
-259-139 -17 154 546 432-278-421 19 131 102 156-165-339 377 974 467-158 -88 -19-101 191 272-166 -11 685 585 -9 -98 -72-259

Figure 11. Zero section of electron density map

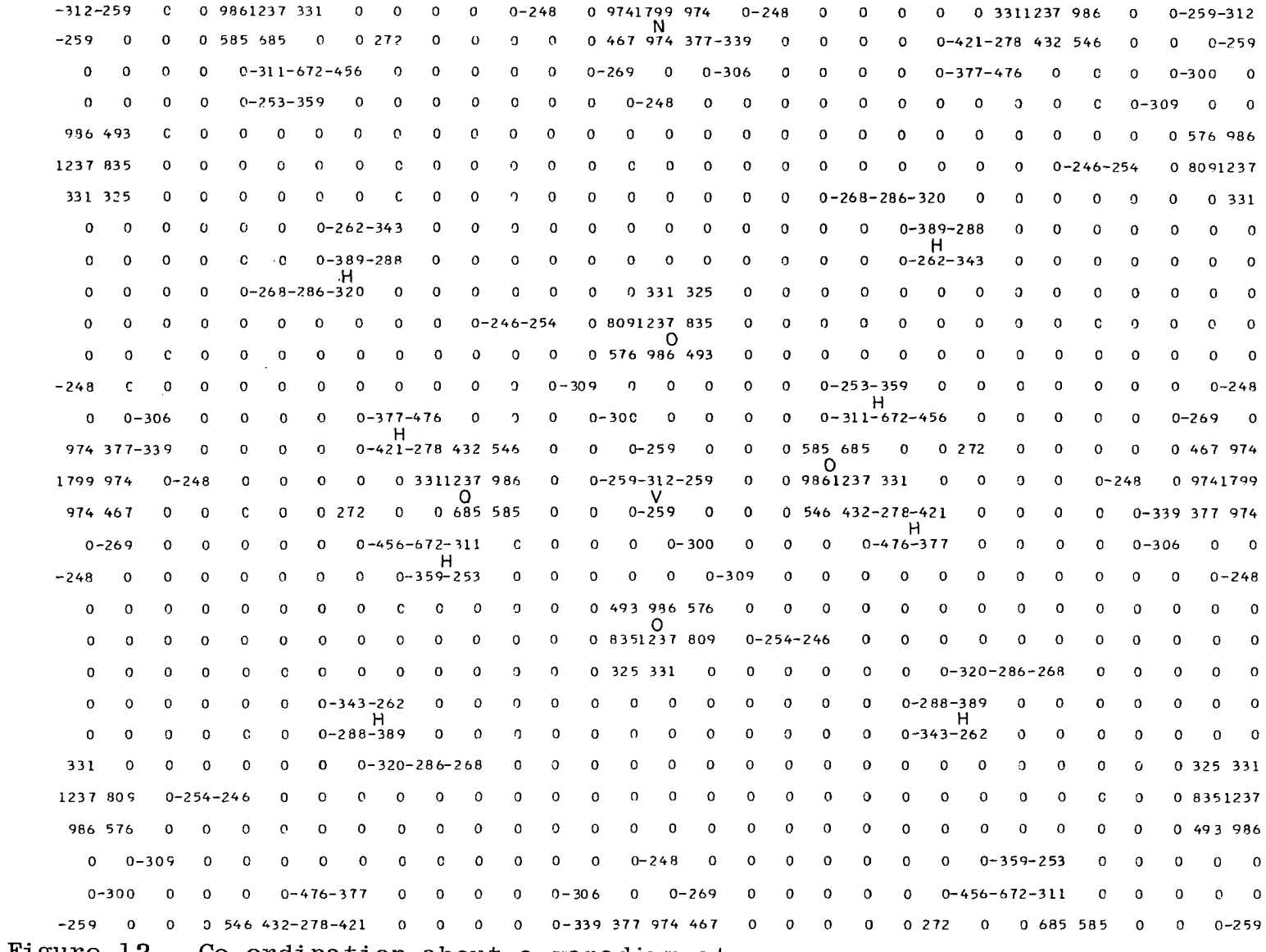

Figure 12. Co-ordination about a vanadium atom

DIRECT METHOD RESEARCH

Direct methods might be described as determination of the phases of the reflections by a mathematical treatment of the intensities. This chapter describes three direct methods and the attempts to apply them to the solution of crystal structures. All three methods depend on a knowledge of positions in the unit cell where there is near-zero electron density. Such positions (called "null-points") can be obtained from a Patterson map by using vector verification (27). Since a Patterson map can be calculated from intensities without regard to phases, null-points can be found without knowledge of phases.

The first method attempted was one proposed by Jacobson[*]. The electron density (ρ) in a centrosymmetric structure at a point (x,y,z) is given by:

$$\rho(x,y,z) = \frac{1}{V} \sum_{h=-\infty}^{\infty} \sum_{k=-\infty}^{\infty} \sum_{\ell=-\infty}^{\infty} F(h,k,\ell)[\cos 2\pi(hx + ky + \ell z)]$$

where $F(h,k,\ell)$ is the structure factor having Miller indices h,k,ℓ, and V is the volume of the unit cell. If we let $\vec{r}=(x,y,z)$ and $\vec{h}=(h,k,\ell)$, then we can write:

$$\rho(\vec{r}) = \frac{1}{V} \sum_{i=1}^{\infty} S(\vec{h}_i)|F(\vec{h}_i)| \cos 2\pi(\vec{h}_i \cdot r)$$

---

[*]Jacobson, R. A. Department of Chemistry, Iowa State University of Science and Technology, Ames, Iowa. Nonclassical direct methods. Private Communication. 1965.

where $S(\vec{h}_i)$ is +1 if $F(\vec{h}_i)$ is positive and -1 if $F(\vec{h}_i)$ is negative.

Let us assume that $\rho(\vec{r})$ can be accurately represented if we use only the n+4 largest structure factors. At a point $(\vec{r})$ where there is no electron density, then

$$\sum_{i=1}^{n+4} S(\vec{h}_i)|F(\vec{h}_i)|\cos 2\pi(\vec{h}_i \cdot \vec{r}) = 0.$$

We know, however, that $F(\vec{0})$ is always positive and that we can pick the signs of three reflections whose Miller indices meet certain conditions. This process of selection merely determines at which of the eight centers of symmetry in the unit cell the origin will be located. Then those four terms can be moved to the other side of the equation, and their sum will be represented by B.

If we pick n points at which $\rho(\vec{r})=0$, we can set up n equations with n unknowns:

$$S(\vec{h}_1)|F(\vec{h}_1)|\cos 2\pi(\vec{h}_1 \cdot \vec{r}_1) + \ldots + S(\vec{h}_n)|F(\vec{h}_n)| \cos 2\pi(\vec{h}_n \cdot \vec{r}_1) = B_1$$

$$\vdots$$

$$S(\vec{h}_1)|F(\vec{h}_1)|\cos 2\pi(\vec{h}_1 \cdot \vec{r}_n) + \ldots + S(\vec{h}_n)|F(\vec{h}_n)| \cos 2\pi(h_n \cdot r_n) = B_n$$

Representing this system of equations in the well known matrix form:

$$FS = B$$

then

$$S = F^{-1}B$$

where

$$S = \begin{pmatrix} S(\vec{h}_1) \\ \vdots \\ S(\vec{h}_n) \end{pmatrix}$$

$$F = \begin{pmatrix} |F(\vec{h}_1)| \cos 2\pi(\vec{h}_1 \cdot \vec{r}_1) & \cdots & |F(\vec{h}_n)| \cos 2\pi(\vec{h}_n \cdot \vec{r}_1) \\ \vdots & & \\ |F(\vec{h}_1)| \cos 2\pi(\vec{h}_1 \cdot \vec{r}_n) & \cdots & |F(\vec{h}_n)| \cos 2\pi(\vec{h}_n \cdot \vec{r}_n) \end{pmatrix}$$

$$B = \begin{pmatrix} B_1 \\ \vdots \\ B_n \end{pmatrix}$$

The only values of S(h) which make physical sense are +1 and -1. However, when this method was used in an attempt to determine the signs of the calculated structure factors of hydrogen floride, the magnitudes of the S(h) obtained from a solution of the set of simultaneous equations differed widely from 1. It appeared that the matrix F was quite ill-conditioned. This, together with the limited precision of the computer, resulted in the matrix inversion being very inaccurate. In fact, in one case when the calculated inverse was multiplied by the original matrix, some of the off-diagonal terms were larger than some of those on the diagonal. If study of this method is to be pursued further, a better method of solving the system of equations must be found, i.e., possibly some way of forcing the magnitudes of all S(h) to be 1.

A method proposed by Jacobson and Wilkes (28) was also investigated. Assume we have n structure factors and m null-points where the value of the electron density function is very small, approximately 0. Therefore, the sum of the electron density over all these points is also approximately 0, and we can write for centric structures:

$$\sum_{j=1}^{m} \sum_{i=1}^{n} S(\vec{h}_i)\,|F(\vec{h}_i)| \cos 2\pi(\vec{h}_i \cdot \vec{r}_j) = 0.$$

Since $F(\vec{0})$ is always positive, and the cosine of zero is +1, we can write:

$$mF(\vec{0}) + S(\vec{h}_2)\,|F(\vec{h}_2)| \sum_{j=1}^{m} \cos 2\pi(\vec{h}_2 \cdot \vec{r}_j)$$

$$+ S(\vec{h}_3)\,|F(\vec{h}_3)| \sum_{j=1}^{m} \cos 2\pi(\vec{h}_3 \cdot \vec{r}_j)$$

$$+ \ldots + S(\vec{h}_n)\,|F(\vec{h}_n)| \sum_{j=1}^{m} \cos 2\pi(\vec{h}_n \cdot \vec{r}_j) = 0.$$

Note that $F(\vec{0})$ is by far the largest structure factor, usually about 3.5 times the size of the second largest reflection. Also note that as we include more and more null-points in the summation, the first term steadily increases while the remaining terms increase much more slowly, since the individual values of the cosine can range from +1 to -1. If enough null-points are included, each term of the type

$$S(\vec{h}_i)\,|F(\vec{h}_i)| \sum_{j=1}^{m} \cos 2\pi(\vec{h}_i \cdot \vec{r}_j)$$

must be negative to counteract the large and positive first term in the equation. Therefore,

$S(\vec{h}_i)$ has a sign which is opposite that of the quantity

$$\sum_{j=1}^{m} \cos 2\pi(\vec{h}_i \cdot \vec{r}_j).$$

This method was used on the structure of HF and gave a high percentage of correct signs when the null-points were taken from an electron density map. However, if the selected points of zero electron density are those which can be determined directly from a Patterson map, the method suffers a severe setback. This is because for centrosymmetric structures, any information obtainable from the Patterson (without superpositions) about the point x,y,z is identical to that obtainable about the seven other points related by translations of 1/2. Then if one or more of the Miller indices is odd, for every null-point which gives rise to a positive term in the cosine summation there is a null-point which gives a negative term of the same magnitude, so that the summation is always zero for such reflections. The method should apply, however, for the 1/8 of the reflections whose indices are all even. In general, this method showed more promise than did the other methods described here.

A direct method proposed by the author was also investigated. If

$$\rho(r)/V = \sum_{h} F(\vec{h}) \cos 2\pi (\vec{h} \cdot \vec{r})$$

then

$$[\rho(\vec{r})/V]^2 = \sum_h [F(\vec{h})]^2 \cos^2 2\pi(\vec{h} \cdot \vec{r})$$

$$+2\sum_{\substack{h \\ h\neq H}} \sum_H F(\vec{h})F(\vec{H}) \cos 2\pi(\vec{h} \cdot \vec{r}) \cos 2\pi(\vec{H} \cdot \vec{r})$$

Let A and B represent these two terms respectively so $[\rho(\vec{r})/V]^2 = A + B$. Now $[\rho(\vec{r})/V]^2 \geq 0$, therefore $A + B \geq 0$ or $A \geq -B$. Since A contains only squared terms, the magnitude of A is independent of the signs of the structure factors. The magnitude of B, however, is not.

At a point where $\rho(\vec{r})=0$, then $[\rho(\vec{r})]^2=0$ and A+B=0 or A=-B. From the above we know that -B can never be greater than A, so if -B=A, -B must be at a maximum. The correct set of signs for the structure factors is therefore one which makes B a minimum.

This method was used in an attempt to predict signs for a few known cases, but no effective method of minimizing B was found. An extension of this method was proposed by Jacobson and investigated by Hansen (29). Difficulties similar to those described here were encountered in that study.

EMULSION CALIBRATION

The work described in this chapter was performed under the direction of Dr. L. S. Bartell, who has since become associated with the University of Michigan.

In electron diffraction, intensities can be recorded on a photographic emulsion which is uniformly spread onto a glass plate. The emulsion contains many tiny crystals of approximately equal size. The usual model (30) explaining the darkening of the plate upon exposure to electrons is that an electron is absorbed by a crystal and that the entire crystal turns black. At first one crystal turns black for every electron striking the plate; therefore initially the optical density of darkness (D) of the plate is proportional to the exposure (E) of the plate, which is defined as the number of electrons having hit the plate per unit area. Let us assume units so that the constant of proportionality is unity; then E=D. When an electron is absorbed by a crystal which is already black, no additional darkening takes place. Obviously, after all the crystals have turned black, the plate can get no darker. The graph in Figure 13 shows the expected relationship of E and D.

At any time the exposure can be given by the infinite series:

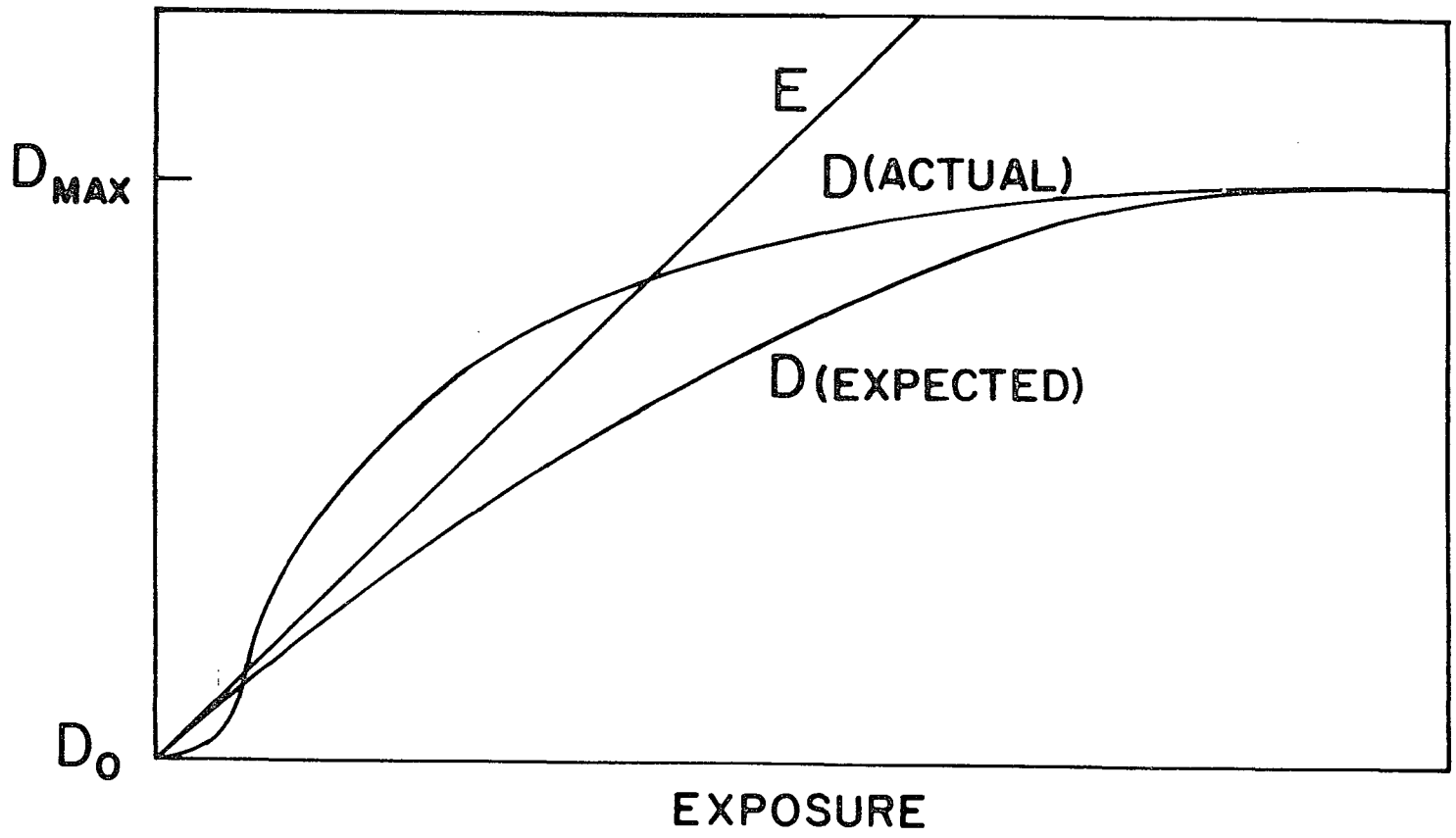

Figure 13. Relation between exposure and darkness

$$E = D + \alpha D^2 + \beta D^3 + \ldots$$

where α and β are constants depending on properties of a particular plate such as Ag crystal size, and the difference between the original darkness (D_o) and maximum darkness (D_{max}). If it is assumed that all terms higher than second order can be neglected, $E = D + \alpha D^2$. The symbol α is called the emulsion constant.

The value for α had in the past been determined by separate experimentation, that is, by using plates which were exposed expressly for emulsion calibration (30). The values obtained had decreased from 0.3 for the plates first (30) used (called lantern slides) to 0.05 for the kind of plates being used (31) when this study began. This decrease was due to improvements in the emulsion, principally decreased crystal size. Since this method of emulsion calibration had recently given spurious results, the author was assigned the problem of finding a new method of emulsion calibration, preferably one which would make use of data taken for structural studies.

If we have two plates (a and b) which have both been exposed in the same manner (that is, electrons of the same energy being diffracted by molecules of the same gas), the ratio of exposure (R) between any two points on different plates which are the same distance from the center of the plate will be constant. The equation

$$R = E_a/E_b = (D_a + \alpha D_a^2)/D_b + \alpha D_b^2) \qquad \text{Equation (1)}$$

must hold for all sets of corresponding points taken from two different plates, even though the darkness differs widely from one point to another on the same plate. It should be pointed out that both α and R are unknowns. Ideally, it would seem that R could be experimentally determined by recording the length of time that the electron beam was on while each plate was being exposed. This cannot be done, however, because of continuous fluctuations in the pressure of the gas which is scattering the electrons.

If the above equation is rearranged using the binomial expansion, we obtain:

$$D_a/D_b = R + \alpha R(D_b - D_a).$$

A plot of D_a/D_b versus $D_b - D_a$ should be a straight line which has an intercept of R and a slope of αR. The value of α can be obtained from such a plot, but it is necessary to use small differences in fairly large numbers and this results in points being widely scattered from the best straight line. Various attempts were made to rearrange this expression so that differences did not need to be used, but in all cases application of the method to data plates met with very limited success. It was then noted that trial and error would be a very simple method of getting an approximate value for α. The "best" value for α would be the one which gives the most nearly constant value for R, as calculated from Equation 1.

This method gave values of α which varied between pairs of plates, but one thing was unmistakeable; α was negative for the range of intensities studied. The estimated value on the basis of this study was -0.05 ± 0.05. This is certainly not predicted by the model described above.

These results prompted a later more complete study at the University of Michigan. That study[*] showed that a plot of D versus E is actually as illustrated in Figure 13.

A model has been developed which would explain such a trend, but it has by no means been proven and requires an assumption which might seem a bit unreasonable. As in the first model, if a crystal stops an electron, it absorbs all of the electron's energy and turns black. Now we assume that a crystal can also absorb some energy from a passing electron without stopping it. The amount of energy absorbed from one electron in this way will not be enough to turn the crystal black, but the energy absorbed from several electrons would be. A crystal which has absorbed some energy but has not turned black will be called "sensitized". Many electrons pass through the emulsion without causing any crystal to turn black, hence initially D is less than E. After a while, however, enough crystals

---

[*]Janzen, J. Department of Chemistry, University of Michigan, Ann Arbor, Michigan. Emulsion Calibration. Private Communication. 1965.

have been sensitized so that one electron can cause more than one crystal to turn black, and D becomes greater than E. Finally, after almost all the crystals have turned black, the optical density levels off at D_{max}.

A second property of the plates which was tested in this study was the uniformity of sensitivity with respect to position of the emulsion on the plate. It was well known that lantern slides were much more sensitive at the edges than at the center and that the effect, if present at all, was not as pronounced in the more modern plates.

To measure this effect, a long narrow box of canvas was constructed. Plates were hung at one end and a light source at the other. The light was activated for short periods of time, never more than a few seconds, and the plates were thought to be very uniformly exposed. The optical density of each plate was recorded with a microphotometer over all of its radius (44 mm) and plotted as a function of radius.

In every case the plates were darker near the edges than at the middle. However, there appeared to be only limited reproducibility in the features of the curves. By averaging densities for many plates the following results were obtained:

1) From the center out to 24 mm, there is little change in density.

2) From 24 to 44 mm, there is approximately 5 $^{o}/_{o}$ increase in optical density.

3) The increase in density goes approximately as the square of (radius-24) mm.

These results, though only approximate, were felt to warrant a correction for intensities as a function of plate position. These numbers are currently being used in corrections for intensities in electron diffraction studies conducted at the University of Michigan.

LITERATURE CITED

1. Cotton, F. A. and G. Wilkinson. J. Am. Chem. Soc. 79: 752. 1957.

2. Sheline, Raymond K. J. Am. Chem. Soc. 73: 1615. 1951.

3. Dahl, Lawrence F. and R. E. Rundle. J. Chem. Phys. 27: 323. 1957.

4. Herber, R. H., W. R. Kingston and G. K. Wertheim. Inorg. Chem. 2: 153. 1963.

5. Dobson, Gerard R. and Raymond K. Sheline. Inorg. Chem. 2: 1313. 1963.

6. Corey, Eugene R. and Lawrence F. Dahl. Inorg. Chem. 1: 521. 1962.

7. Dahl, Lawrence F. and R. E. Rundle. J. Chem. Phys. 26: 1751. 1957.

8. Dahl, Lawrence F. and John F. Blount. Inorg. Chem. 4: 1373. 1965.

9. Angelici, Robert J. and E. Edwin Siefert. Inorg. Chem. 5: 1457. 1966.

10. Dahm, Donald J. and Robert A. Jacobson. Chem. Comm. 496. 1966.

11. Wei, Chin Hsuan and Lawrence F. Dahl. J. Am. Chem. Soc. 88: 1821. 1966.

12. Hoard, Laurence G. and Robert A. Jacobson. J. Chem. Soc. (A) 1203. 1966.

13. Jacobson, Robert A., Jeffrey A. Wunderlich and William N. Lipscomb. Acta Cryst. 14: 598. 1961.

14. Howells, E. R., D. C. Phillips and D. Rogers. Acta Cryst. 3: 210. 1950.

15. Karle, Isabella L. and J. Karle. Acta Cryst. 16: 969. 1963.

16. Mills, O. S. Acta Cryst. 11: 620. 1958.

17. Powell, H. M. and R. V. G. Ewens. J. Chem. Soc. 286. 1939.

18. Cotton, F. A. and G. Wilkinson. Advanced inorganic chemistry. New York, N.Y., Interscience Publishers. 1967.

19. Angelici, Robert J. and Mary Diana Malone. Inorg. Chem. 6: 1731. 1967.

20. Kettle, S. F. A. Inorg. Chem. 4: 1661. 1965.

21. Eyring, Henry, John Walter and George E. Kimball. Quantum chemistry. New York, N.Y., John Wiley and Sons, Inc. 1954.

22. Dahm, D. J., J. E. Benson, D. M. Nimrod, D. R. Fitzwater and R. A. Jacobson. U.S. Atomic Energy Commission Report IS-1701 [Iowa State University of Science and Technology, Ames. Inst. for Atomic Research]. 1967.

23. Fitzwater, D. R. and D. E. McFarland. U.S. Atomic Energy Commission Report IS-1280 [Iowa State University of Science and Technology, Ames. Inst. for Atomic Research]. 1965.

24. Fitzwater, D. R., D. E. McFarland and C. E. Runge. U.S. Atomic Energy Commission Report IS-1279 [Iowa State University of Science and Technology, Ames. Inst. for Atomic Research]. 1965.

25. Larson, Allen C. and Don T. Cromer. Acta Cryst. 22: 793. 1967.

26. Bacon, G. E. and W. E. Gardner. Proc. Roy. Soc. 246: 78. 1958.

27. Mighell, Alan D. and Robert A. Jacobson. Acta Cryst. 16: 443. 1963.

28. Wilkes, Charles Eugene. The crystal and molecular structures of di-μ-diphenylphosphinatoacetylacetonato chromium(III) and tetrakis (ethylenediamine)-μ-amido-μ-nitrodicobalt(III) nitrate, balanced filters, multiple-vector superpositions, and some direct methods. Unpublished Ph.D. thesis. Princeton, New Jersey, Library, Princeton University. 1964.

29. Hansen, Peter Jacob. The crystal structure determination of π-$C_5H_5Fe(CO)_2Mn(CO)_5$. Unpublished Ph.D. thesis. Ames, Iowa, Library, Iowa State University of Science and Technology. 1966.

30. Bartell, L. S. and L. O. Brockway. J. Appl. Phys. 24: 656. 1953.

31. Bartell, L. S., Kozo Kuchitsu and R. J. de Neui. J. Chem. Phys. 35: 1211. 1961.